

One-loop corrections to polarization observables

J.G. Körner¹ and M.C. Mauser

Institut für Physik, Johannes Gutenberg-Universität
Staudinger Weg 7, D-55099 Mainz, Germany

Abstract

We review the physics of polarization observables in high energy reactions in general and discuss the status of *NLO* one-loop corrections to these observables in specific. Many high order radiative corrections exist for rates but not many *NLO* radiative corrections exist for polarization observables. The radiative correction calculations for polarization observables are somewhat more complicated than those for rates. They tend to be smaller than those for the rates. In most of the examples we discuss we include mass effects which significantly complicate the radiative correction calculations. We elaborate a general scheme which allows one to enumerate the number of independent density matrix elements in a reaction and provide explicit examples of angular decay distributions in self-analyzing decays that allow one to experimentally measure the density matrix elements. We provide examples of reactions where certain density matrix elements are only populated at *NLO* or by mass effects. In our discussion we concentrate on semileptonic bottom and top quark decays which are linked to leptonic μ and τ decays through a Fierz transformation.

¹ *Invited lecture at the International School “Heavy Quark Physics”,
Dubna, Russia, 27 May – 5 June 2002
To appear in the Proceedings (Lecture Notes in Physics)*

1 Introduction

Most of the *NLO* radiative corrections to rates have been done quite some years ago. In fact, two-loop *NNLO* calculations for rates are now becoming quite standard. In e^+e^- annihilation one is even pushing hard to determine the *NNNNLO* corrections to the R ratio [1, 2]. Contrary to this, many *NLO* radiative correction calculations to polarization observables involving also massive quarks have only been done in the last few years.

It is clear that higher order radiative corrections to unpolarized observables will always be at the center of attention because data on unpolarized observables are as a rule much more accurate than data for polarized observables. Nevertheless, as experimental data on polarization observables has been accumulating over the years there is an evolving need for radiative corrections to polarization observables. One of the reasons that polarized radiative correction were lagging behind unpolarized radiative corrections is that the computational effort in the calculation of radiative corrections to polarization observables is larger than that for rates. For once, one cannot sum over the spins of intermediate states whose polarization one wants to calculate. One therefore cannot make use of the powerful unitarity method to calculate radiative corrections from the absorptive parts of higher order loop graphs. Further, the definition of polarization observables brings in extra momentum factors in the integrands of the requisite phase space integrals which makes life more difficult. This is particularly true if the masses of particles in the process cannot be neglected. For example, in the process $t \rightarrow b + W^+$ the longitudinal component of the polarization vector of the top quark along the W -direction is given by

$$s_t^{l,\mu} = \frac{1}{|\vec{q}|} \left(q^\mu - \frac{p_t \cdot q}{m_t^2} p_t^\mu \right), \quad (1)$$

where the denominator factor $|\vec{q}| = \sqrt{q_0^2 - m_W^2}$ comes in for normalization reasons (q is the momentum of the W^+). It is quite clear that such square root factors lead to nontrivial complications in the phase space integrations. Similar square root factors appear when projecting onto the polarization states of the W^+ .

Inclusion of mass effects as e.g. in the semileptonic decay $b \rightarrow c + l^- + \bar{\nu}_l$ ($m_c/m_b \approx 0.30$) or in the leptonic decay $\tau^- \rightarrow \mu^- + \nu_\tau + \bar{\nu}_\mu$ ($m_\mu/m_\tau \approx 0.07$) render the analytical calculations considerably more complicated. The villain is the Källén function $(m_1^4 + m_2^4 + m_3^4 - 2(m_1^2 m_2^2 + m_1^2 m_3^2 + m_2^2 m_3^2))^{1/2}$ which is brought in by extra three-momentum factors. In the case that e.g. $m_3 \rightarrow 0$ the Källén function simplifies to $(m_1 - m_2)^2$ which leads to an enormous simplification in the phase space integrals.

Physically speaking mass effects become large in regions of phase space where the massive particles become nonrelativistic. For example, in the leptonic decay of the muon

$\mu^- \rightarrow e^- + \nu_\mu + \bar{\nu}_e$, the mass of the electron cannot be neglected in the threshold region where the energy of the electron is small. This is illustrated in Fig. 1 where the longitudinal polarization of the electron is plotted against the scaled energy $x = 2E_e/m_\mu$ of the electron [3]. We have chosen a logarithmic scale for x in order to enhance the threshold region. In the threshold region the longitudinal polarization deviates considerably from the naive value $P_e^l = -1$. The radiative corrections in the threshold region can be seen to be quite large.

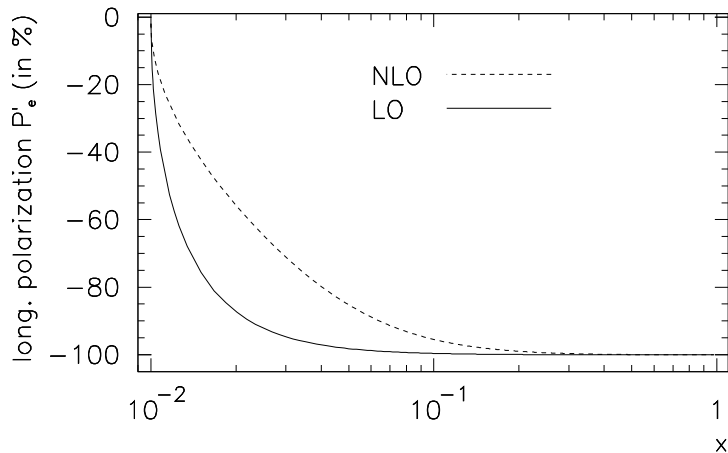


Figure 1: Longitudinal polarization of the electron in leptonic muon decays at LO and NLO as a function of the scaled energy $x = 2E_e/m_\mu$ [3]. The LO curve is very well described by the functional behaviour $P_e^l = -\beta$.

All our results are given in closed analytic form. In the days of fast numerical computers one may rightfully ask what the advantage of having closed form expressions is. One of the advantages is that all requisite mass and momentum limits can be taken in analytic form. Thus the analytic results can be subjected to tests against known limiting cases providing for the necessary checks of the full results. A second issue is user-friendliness. The analytic expressions are simple enough to be incorporated in numerical programs by the prospective user. Parameter values such as masses and coupling constants can be varied at will by the user in his own program without having to refer to numerical programs written by others. We have checked that our analytical formulas are numerically stable even in the small and large mass limits.

NLO corrections to rates can be quite large. NLO corrections to polarization observables have a tendency to be somewhat smaller. The reason is that polarization observables

are normalized quantities. They are normalized with regard to the total rate. The numerators and denominators in the relevant polarization expressions tend to go in the same direction. The reason is that the *NLO* numerators and denominators are dominated by the soft gluon or soft photon contributions which are universal in the sense that they multiply the relevant Born term expressions and thus cancel out in the ratio. For example, for $t \rightarrow b + W^+$ the $O(\alpha_s)$ correction to the rate is -8.5% and $(-2.5\% \div +3\%)$ for the polarization observables [4, 5, 6].

At *NLO* some density matrix elements become populated which vanish at leading order. An example is again the decay $t \rightarrow b + W^+$ where the rate into the right-handed W^+ vanishes ($\Gamma(W_R) = 0$) for $m_b = 0$ at *LO* but where $\Gamma(W_R) \neq 0$ at *NLO*. Generally speaking, Standard Model radiative corrections can populate density matrix elements that vanish at leading order. Consequently radiative corrections change angular decay distributions as do new physics effects. The lesson to be learned is clear. Before ascribing a given polarization effect to new physics one has to make sure that it does not result from radiative corrections of old physics. In the above example a non-zero $\Gamma(W_R) \neq 0$ could result from an admixture of a right-handed charged current (new physics) or from radiative corrections. Only the precise knowledge of the magnitude of the radiative corrections allows one to exclude or conclude for new physics effects.

In this review we will mostly be concerned with radiative corrections to the current-induced transitions $t \rightarrow b$, $b \rightarrow c$ and $l \rightarrow l'$. It should be clear that the additional gluons (or photons) in radiative correction calculations only couple to the $q_1 \rightarrow q_2$ (or $l \rightarrow l'$) side of the relevant semileptonic (or leptonic) transitions. This implies that the structure of the *NLO* radiative corrections is the same in the two classes of processes. The current-induced transition $l \rightarrow l'$ is not in the Standard Model form but in the charge retention form. However, the charge retention form can be linked to the Standard Model form by the remarkable property that the $(V - A)^\mu(V - A)_\mu$ interaction is an eigenvector under Fierz crossing (see Sect. 3). One therefore has

$$\mathcal{L} = \frac{G_F}{\sqrt{2}} [\bar{\nu}_\mu \gamma^\alpha (\mathbb{1} - \gamma_5) \mu] [\bar{e} \gamma_\alpha (\mathbb{1} - \gamma_5) \nu_e] + \text{h.c.} \quad (2)$$

$$= \frac{G_F}{\sqrt{2}} [\bar{\nu}_\mu \gamma^\alpha (\mathbb{1} - \gamma_5) \nu_e] [\bar{e} \gamma_\alpha (\mathbb{1} - \gamma_5) \mu] + \text{h.c.} \quad (3)$$

All of the above three transitions are therefore governed by the same matrix elements. In particular the *NLO* QED and QCD radiative corrections have the same structure for all three transitions. In Table 1 we provide a list of the processes for which the radiative corrections to the rates and the polarization observables can all be calculated

Table 1: List of processes based on the same current-induced matrix elements

parton level	particle level	references
$t(\uparrow) \longrightarrow b + W^+(\uparrow)$	$t(\uparrow) \longrightarrow X_b + W^+(\uparrow)(\longrightarrow l^+ + \nu_l)$	[4, 5, 6, 7]
$t(\uparrow) \longrightarrow b + H^+$	$t(\uparrow) \longrightarrow X_b + H^+$	[8]
$b(\uparrow) \longrightarrow c(\uparrow) + l^- + \bar{\nu}_l$	$B \longrightarrow X_c + D_s^{(*)}(\uparrow)$	[9]
	$\Lambda_b(\uparrow) \longrightarrow X_c + D_s^{(*)}(\uparrow)$	[10]
$b(\uparrow) \longrightarrow u(\uparrow) + l^- + \bar{\nu}_l$	$B \longrightarrow X_u + \pi(\rho(\uparrow))$	[9]
	$\Lambda_b(\uparrow) \longrightarrow X_u + \pi(\rho(\uparrow))$	[10]
$l^-(\uparrow) \longrightarrow l'^-(\uparrow) + \nu_l + \bar{\nu}_{l'}$		[3]
$(l, l') = (\mu, e), (\tau, \mu), (\tau, e)$		

from essentially the same set of *NLO* matrix elements. In this review we shall only present a few sample results from the processes in Table 1 because the results are too numerous to fit into a review of the present size. Instead we attempt to share our insights into the general features of spin physics and illustrate these with sample results taken from the processes in Table 1.

2 Miscellaneous Remarks on Polarization Effects

2.1 Examples of 100% polarization

In this subsection we discuss examples of 100% polarization. Cases of 100% polarization are usually associated with limits when masses or energies of particles become small or large compared to a given scale in a process. For example, an on-shell or off-shell gauge bosons radiated off massless fermions (leptons or quarks) is purely transverse since fermion helicity is conserved by the vector and axial vector Standard Model couplings of the gauge bosons. Contrary to this, massive gauge bosons become purely longitudinal in the high energy limit (see Sect. 11). We discuss two examples of 100% polarization in more detail. Namely, the case of a left-chiral fermion which becomes purely left-handed in the chiral limit when $m_f \rightarrow 0$ and the case of soft gluon radiation from heavy quarks.

Relativistic left–chiral fermions

Consider a fermion moving along the z -axis. The positive and negative helicity polarization four–vectors of the fermion are given by $s_{\pm}^{\mu} = \pm(p; 0, 0, E)/m$. At first sight it appears to be problematic to take the limit $m \rightarrow 0$ in expressions involving the polarization four–vectors because of the denominator mass factor. However, the saving feature is that s_{\pm}^{μ} becomes increasingly parallel to the momentum $\pm p^{\mu}$ when $m \rightarrow 0$. In fact, one has

$$s_{\pm}^{\mu} = \pm p^{\mu} + O(m/E), \quad (4)$$

since $E = p + (m^2)/(E + p)$. Therefore the projectors onto the two helicity states simplify to

$$u(\pm)\bar{u}(\pm) = \frac{1}{2}(\not{p} + m)(\mathbb{1} + \gamma_5 \not{s}_{\pm}) \xrightarrow{m \rightarrow 0} \frac{1}{2}\not{p}(\mathbb{1} \mp \gamma_5). \quad (5)$$

This shows that a right/left–chiral fermion is purely right/left–handed in the chiral limit. Thus the final state electron emerging from leptonic μ -decay is purely left–handed in the chiral limit except for the anomalous spin–flip contribution appearing first at NLO which populate also the right–handed state. The anomalous spin–flip contribution will be discussed in Sect. 12.

The approach to the chiral limit is well described by an approximate formula frequently discussed in text books. The argument goes as follows.

Introduce left–chiral fermion spinors according to $u_L(\pm) = 1/2(\mathbb{1} - \gamma_5)u(\pm)$, where $u(\pm)$ are helicity $\lambda = +1/2, -1/2$ spinors. The longitudinal polarization of a left–chiral electron is then calculated by taking the ratio of the difference and the sum of the $\lambda = +1/2$ and $\lambda = -1/2$ scalar densities according to

$$P_e^l = \frac{u_L^{\dagger}(+)u_L(+) - u_L^{\dagger}(-)u_L(-)}{u_L^{\dagger}(+)u_L(+) + u_L^{\dagger}(-)u_L(-)} \quad (6)$$

$$= \frac{(E + m - p)^2 - (E + m + p)^2}{(E + m - p)^2 + (E + m + p)^2} = -\frac{p}{E} = -\beta. \quad (7)$$

A corresponding result holds for left–chiral positrons where $P_e^l = \beta$.

The accuracy of the above result can be checked with the corresponding expression for the Born term polarization of the electron in leptonic μ -decay. One finds (see e.g. [3])

$$P_e^l = -\beta \frac{x(3 - 2x + y^2)}{x(3 - 2x) - (4 - 3x)y^2}, \quad (8)$$

where $x = 2E_e/m_\mu$ and $y = m_e/m_\mu$. For the Born term contribution the correction to the approximate result (6) $P_e^l = -\beta$ is of $O(1\%)$ or less such that the correct and approximate curves are not discernible at the scale of Fig. 1. Contrary to this the *NLO* polarization deviates substantially from a simple $P_e^l = -\beta$ behaviour (see Fig. 1) even though one has again $P_e^l \propto -\beta$ at *NLO* [3]. This may have to do with the fact that the radiative corrections involve an extra photon emission from the electron leg. The electron is therefore no longer left-chiral at *NLO* as in the *LO* Born term case.

Soft gluon or soft photon radiation

When a soft gluon (or a soft photon) is radiated off a fermion line it is 100% polarized in the plane spanned by the fermion and the gluon (or photon). To see this in an exemplary way consider the tree graph matrix element of a soft gluon radiated off a top or antitop in the process $e^+e^- \rightarrow t\bar{t}g$. The soft gluon matrix element reads

$$T_\mu^{(\text{s.g.})}(\pm) = T_\mu^{(\text{Born})} \left(\frac{p_t^\alpha}{p_t \cdot k} - \frac{p_{\bar{t}}^\alpha}{p_{\bar{t}} \cdot k} \right) \epsilon_\alpha^*(\pm) \quad (9)$$

with $\epsilon_\alpha^*(\pm) = (0; \mp 1, i, 0)/\sqrt{2}$.

The 2×2 density matrix of the gluon can be expanded in terms of the unit matrix $\mathbb{1}$ and the Pauli matrices σ_i according to

$$\begin{pmatrix} h_+ h_+^* & h_+ h_-^* \\ h_- h_+^* & h_- h_-^* \end{pmatrix} = \frac{1}{2} (\sigma \cdot \mathbb{1} + \vec{\xi} \cdot \vec{\sigma}), \quad (10)$$

where $\vec{\xi}$ denotes the Stokes “vector”. We have set “vector” in quotation marks because the Stokes “vector” does not transform as a vector but rather as a spin 2 object under three-dimensional rotations. From (9) one sees that the helicity amplitudes are relatively real and that $h_+ = -h_-$. The normalized Stokes “vector” is then given by

$$\vec{\xi}/\sigma = (-1, 0, 0), \quad (11)$$

i.e., in the terminology of classifying the polarization states of a gluon (or a photon), the polarization of the gluon is 100% linearly polarized in the production plane.

In Fig. 2 we show a plot of the linear polarization of the gluon as a function of the scaled energy of the gluon for $e^+e^- \rightarrow t\bar{t}g$ and for $e^+e^- \rightarrow c\bar{c}g$ [11]. At the soft end of the spectrum the gluon is 100% polarized and then slowly drops to zero polarization at the hard end of the spectrum. It is quite remarkable that a high degree of polarization is maintained over a large part of the spectrum.

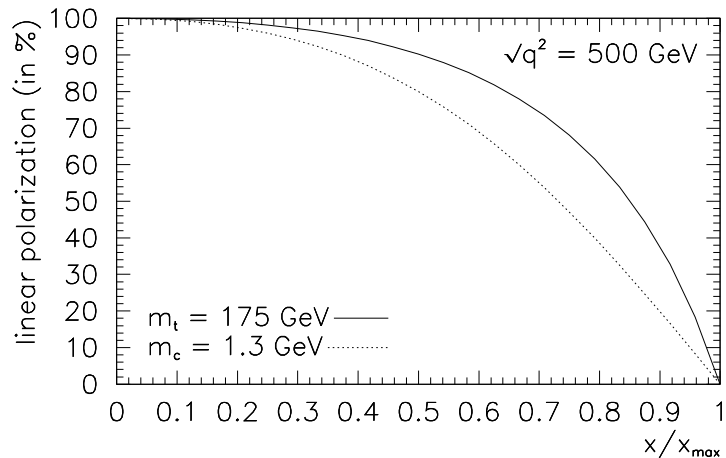


Figure 2: Linear polarization of the gluon as a function of the scaled energy of the gluon in $e^+e^- \rightarrow Q\bar{Q}g$ [11].

2.2 Examples of zero polarization

The mean of a single spin polarization observable such as $\langle \vec{\sigma} \cdot \vec{p} \rangle$ is a parity-odd measure. In strong interaction processes, which are parity conserving, there are no single spin polarization effects, i.e. $\langle \vec{\sigma} \cdot \vec{p} \rangle = 0$ (except for the T -odd single spin effects $\propto \langle \vec{\sigma} \cdot (\vec{p}_i \times \vec{p}_j) \rangle$ to be discussed later on). This is different in weak and electroweak interactions where the presence of parity violations induces a wide variety of single spin polarization phenomena. As an example we take e^+e^- -annihilation into heavy quarks where single spin polarization phenomena occur due to (γ, Z) -exchange. NLO corrections to these single spin polarization phenomena have been discussed in [12, 13, 14, 15, 16, 17]. Another example is the semileptonic decay of a polarized heavy quark where the NLO corrections to the lepton spectrum have been presented in [18, 19].

However, there are double spin polarization effects in strong interactions since $\langle \vec{\sigma} \cdot \vec{\sigma} \rangle$ is a parity even measure. An example is the correlation between the spins of the top and the antitop produced in hadronic collisions [20, 21, 22, 23]. Naturally, double spin polarization effects also occur in weak interaction processes such as in high energy e^+e^- -annihilation (see [16, 24, 25, 26]). However, even in weak processes single spin polarization effects can vanish when one approaches phase space boundaries. Consider, for example, the process $e^+e^- \rightarrow t\bar{t}$ at threshold. In general, the vector current induced amplitude is s - and d -wave, while the axial vector current amplitude is p -wave. As one approaches threshold the s -wave amplitude will dominate and thus there will be no vector-axial

vector interference. Therefore single top polarization goes to zero in $e^+e^- \rightarrow t\bar{t}$ as one approaches the threshold region.

Another example of zero polarization are *NLO* T -odd measures in the process $e^+e^- \rightarrow q\bar{q}(g)$ for massless quarks. T -odd effects arise from the imaginary parts of one-loop contributions. However, in the case $e^+e^- \rightarrow q\bar{q}(g)$ the imaginary parts can be shown to be proportional to the Born term contribution in the mass zero limit. Hence, the T -odd measures are zero in this case [27]. When $m_q \neq 0$ the imaginary parts are no longer proportional to the Born term and, consequently, one obtains nonzero values for the T -odd measures [28, 29]. In the crossed channels (deep inelastic scattering, Drell–Yan process) the imaginary parts no longer have Born term structure and one obtains non-vanishing T -odd effects even for zero mass quarks [30, 31, 32, 33].

2.3 Mass effects

Mass effects make the radiative correction more complicated. We attempt to illustrate the complication brought about by an additional mass scale by listing the (*LO* + *NLO*) results for the total rate of leptonic μ decays $\mu^- \rightarrow e^- + \bar{\nu}_e + \nu_\mu$ for (i) $y = m_e/m_\mu = 0$ and for (ii) $y = m_e/m_\mu \neq 0$. In case (i) one has

$$\Gamma = \frac{G_F^2 m_\mu^5}{192\pi^3} \left(1 + \frac{\alpha}{\pi} \left\{ \frac{25 - 4\pi^2}{8} \right\} \right). \quad (12)$$

For case (ii) one obtains

$$\begin{aligned} \Gamma &= \frac{G_F^2 m_\mu^5}{192\pi^3} \left((1 - y^4)(1 - 8y^2 + y^4) - 12y^4 \ln(y) + \frac{\alpha}{\pi} \left\{ \right. \right. \\ &+ \frac{1}{24}(1 - y^4)(75 - 956y^2 + 75y^4) - 2y^4(36 + y^4) \ln^2(y) \\ &- \frac{\pi^2}{2}(1 - 32y^3 + 16y^4 - 32y^5 + y^8) \\ &- \frac{1}{3}(60 + 270y^2 - 4y^4 + 17y^6)y^2 \ln(y) \\ &- \frac{1}{6}(1 - y^4)(17 - 64y^2 + 17y^4) \ln(1 - y^2) \\ &+ 4(1 - y)^4(1 + 4y + 10y^2 + 4y^3 + y^4) \ln(1 - y) \ln(y) \\ &+ \left. \left. 4(1 + y)^4(1 - 4y + 10y^2 - 4y^3 + y^4) \ln(1 + y) \ln(y) \right\} \right) \end{aligned}$$

$$\begin{aligned}
& + 2(3 + 32y^3 + 48y^4 + 32y^5 + 3y^8)\text{Li}_2(-y) \\
& + 2(3 - 32y^3 + 48y^4 - 32y^5 + 3y^8)\text{Li}_2(y) \Big\}. \tag{13}
\end{aligned}$$

The length of the *NLO* term in (13) illustrates but does not describe the added complication when introducing a new mass scale. The inclusion of full mass effects is not of much relevance for leptonic $\mu^- \rightarrow e^-$ decays (except in the threshold region) where $(m_e/m_\mu)^2 = 2.34 \cdot 10^{-5}$ but may be relevant for the leptonic $\tau \rightarrow \mu$ decays, where e.g. $(m_\mu/m_\tau)^2 = 3.54 \cdot 10^{-3}$. In fact, experimental data on leptonic τ decays do show a mass dependence of the partial rates on the daughter lepton's mass. For the decays $\tau^- \rightarrow \mu^- + \bar{\nu}_\mu + \nu_\tau$ and $\tau^- \rightarrow e^- + \bar{\nu}_e + \nu_\tau$ one finds branching ratios of $17.37 \pm 0.06\%$ and $17.84 \pm 0.06\%$ [34]. In agreement with experiment the *LO* result predicts a reduction of the partial rate by 2.82% for the $\tau^- \rightarrow \mu^-$ mode relative to the $\tau^- \rightarrow e^-$ mode. As concerns *NLO* effects, the experimental errors on the two partial rates are still too large to allow for checks on the mass dependence of the *NLO* result. Quite naturally, for semileptonic $b \rightarrow c$ decays, where $y = m_c/m_b \approx 0.3$, the mass dependence of the daughter quark must be kept.

Mass effects also populate density matrix elements which are zero when a given mass is set to zero. A prominent example is again $e^+e^- \rightarrow q\bar{q}$ which is purely transverse for mass zero quarks but acquires a longitudinal component when the quark becomes massive. In the same vein one has the Callan–Gross relation $F_2 = xF_1$ in deep inelastic scattering for mass zero quarks which is spoiled when the quarks become massive. Another example is the density matrix of the electron in leptonic muon decay. Its off–diagonal elements contribute to the transverse component of the electron's polarization (see (20)). The off–diagonal elements are proportional to the positive helicity amplitude $h_{1/2}$ which in turn is proportional to the mass of the electron ($h_{1/2} \sim m_e$). One therefore has $P_e^\perp \sim m_e$ [3]. A third example is the transition of the top quark into a right–handed W^+ (W_R) and a bottom quark. For $m_b = 0$ the left–chiral bottom quark becomes purely left–handed and, from angular momentum conservation, one therefore finds $\Gamma(W_R) = 0$ (see Fig. 3) (see e.g. [5]).

2.4 Some polarization measures are *NLO* effects

Whenever a given polarization component is zero at the *LO* Born term level, and the vanishing of this polarization component is not due to general symmetry principles, it is very likely that this polarization component will be populated by gluon or photon emission at *NLO*. We shall list a few examples where this is the case.

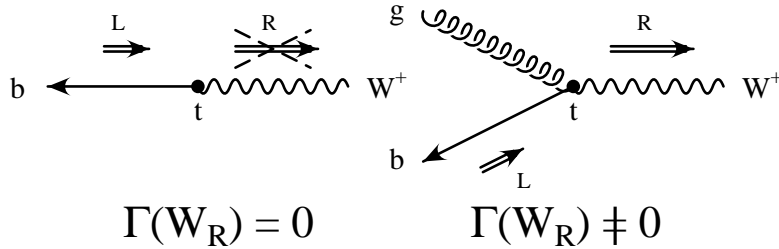


Figure 3: The decay $t \rightarrow b + W_R^+$ at LO and NLO

A prominent example is the Callan–Gross relation which is violated by gluon emission at NLO . Similarly, a longitudinal contribution is generated in e^+e^- -annihilation into massless quarks by gluon emission. T -odd measures derive from imaginary parts of one-loop contributions, i.e. they start only at NLO . As mentioned before, a transverse-plus polarization of the W^+ in the decay $t \rightarrow b + W^+$ is generated by gluon emission as illustrated in Fig. 3. At LO the longitudinal polarization of massive quarks in $e^+e^- \rightarrow Q\bar{Q}$ is purely transverse, i.e. the polar distribution of this polarization component is proportional to $(1 + \cos^2 \theta)$. The appearance of a longitudinal dependence proportional to $\sin^2 \theta$ is a NLO effect [13]. Anomalous helicity flip contributions involving massless quarks or leptons occur only at NLO as discussed in Sect. 12.

We have already mentioned the T -odd measures which, in a CP invariant theory, obtain contributions only from the imaginary parts of NLO one-loop contributions. Apart from the examples listed in Sect. 2.2 we mention the case of the transverse polarization of a top quark produced in hadronic collisions [35, 36, 37].

2.5 Presentation of NLO results of polarization observables

We have always chosen to present our analytical and numerical NLO results on polarization observables in the form

$$\langle P \rangle = \frac{N}{D} = \frac{N^{\text{LO}}(1 + \alpha_s \hat{N}^{\text{NLO}})}{D^{\text{LO}}(1 + \alpha_s \hat{D}^{\text{NLO}})}, \quad (14)$$

and not as

$$\langle P \rangle = \frac{N^{\text{LO}}}{D^{\text{LO}}}(1 + \alpha_s(\hat{N}^{\text{NLO}} - \hat{D}^{\text{NLO}})). \quad (15)$$

An argument for our preference of the form (14) over (15) is the following. It is common usage to try and extend a perturbation series beyond a given known order by Padé improving the perturbation series. For example, for a second order perturbation series the Padé $P(1,1)$ improvement reads

$$1 + \alpha_s a_1 + \alpha_s^2 a_2 \approx \frac{1 + \alpha_s \frac{a_1^2 - a_2}{a_1}}{1 - \alpha_s \frac{a_2}{a_1}}. \quad (16)$$

What has been done in the Padé $P(1,1)$ improvement is to fix the first order coefficients in the numerator and denominator of the r.h.s. of (16) by expanding the r.h.s. in powers of α_s and then equating coefficients in (16). Note that at the NLO level Padé's method does not yet allow one to reconstruct (14) from (15). Considering the successes of the Padé improvement program in other applications we nevertheless believe that the form (14) is a better approximation to the whole perturbation series than (15).

As an example where the use of the form (15) can lead to a misunderstanding is the NLO result of the mean forward–backward asymmetry $\langle A_{\text{FB}} \rangle$ in e^+e^- -annihilation into a pair of massless quarks which, when using the form (15), is sometimes stated as

$$\langle A_{\text{FB}} \rangle = \frac{\sigma_{\text{FB}}^{\text{LO}}}{\sigma^{\text{LO}}} (1 - \alpha_s/\pi). \quad (17)$$

This result is very suggestive of a de facto non-vanishing radiative correction to σ_{FB} . However, the true result is $\sigma_{\text{FB}}^{\text{NLO}} = 0$ [38]. The non-vanishing radiative correction to $\langle A_{\text{FB}} \rangle$ in (17) is just a reflection of the well-known NLO result for the rate $\sigma = \sigma^{\text{LO}}(1 + \alpha_s/\pi)$ in the denominator of (14). To our knowledge the vanishing of $\sigma_{\text{FB}}^{\text{NLO}}$ evades a simple explanation and must be termed to be a dynamical accident.

3 Fierz Transformation

Fierz crossing exchanges two Dirac indices in the contracted product of two strings of Γ -matrices according to (i not summed)

$$[\Gamma_i^{\{\mu\}}]_{\alpha\beta} [\Gamma_{i\{\mu\}}]_{\gamma\delta} \rightarrow [\Gamma_i^{\{\mu\}}]_{\alpha\delta} [\Gamma_{i\{\mu\}}]_{\gamma\beta}, \quad (18)$$

where the five currents in the set are conventionally labelled by $i = S, V, T, A, P$ with $\Gamma_i^{\{\mu\}} = \{1, \gamma^\mu, \sigma^{\mu\nu}, \gamma^\mu\gamma_5, \gamma_5\}$. The set of crossed configurations can then be expressed in terms of the set of uncrossed configurations. The five-by-five matrix relating the two sets is called the Fierz crossing matrix C_{Fierz} . It is clear that one gets back to the original configuration when crossing twice, i.e. $C_{\text{Fierz}}^2 = 1$. The eigenvalues λ of the Fierz crossing

matrix are thus $\lambda = \pm 1$ as can easily be seen by going to the diagonal representation. In explicit form the Fierz crossing matrix is given by

$$C_{Fierz} = \frac{1}{4} \begin{pmatrix} 1 & 1 & 1/2 & -1 & 1 \\ 4 & -2 & 0 & -2 & -4 \\ 12 & 0 & -2 & 0 & 12 \\ -4 & -2 & 0 & -2 & 4 \\ 1 & -1 & 1/2 & 1 & 1 \end{pmatrix}, \quad (19)$$

where the rows and columns are labeled in the order $i = S, V, T, A, P$.

As (19) shows the trace of the Fierz crossing matrix is $Tr(C_{Fierz}) = -1$. This implies that the Fierz crossing matrix has three eigenvalues $\lambda = -1$ and two eigenvalues $\lambda = +1$. When discussing physics applications one also needs the corresponding Fierz crossing matrix for parity odd products of currents. This can easily be derived from multiplying the parity even case by γ_5 .

Amazingly, the charged current interaction of the Standard Model $(V - A)_\mu(V - A)^\mu$ is an eigenvector of Fierz crossing, with eigenvalue $\lambda = -1$. When relating the Standard Model and charge retention forms of the Lagrangian as in (2) the minus sign from Fierz crossing is cancelled from having to commute the Fermion fields an odd number of times in order to relate the two forms.

In pre-QCD days it was considered unfortunate that the eigenvalue of the $(V - A)_\mu(V - A)^\mu$ current-current product is negative. If it were positive one would have a very natural explanation of the so called $\Delta I = 1/2$ - or octet rule in weak nonleptonic decays. To see this consider the direct products $\mathbf{3} \otimes \mathbf{3} = \bar{\mathbf{3}}_a \oplus \mathbf{6}_s$ and $\bar{\mathbf{3}} \otimes \bar{\mathbf{3}} = \mathbf{3}_a \oplus \bar{\mathbf{6}}_s$. With the wrong eigenvalue $\lambda = +1$ (and the minus sign from Fermi statistics) one would then remain with $\bar{\mathbf{3}}_a \oplus \mathbf{3}_a = \mathbf{1} \oplus \mathbf{8}$ and one thus would have explained the famous octet rule for nonleptonic weak interactions. Nevertheless, with the advent of QCD and colour, it was realized that an important class of diagrams in nonleptonic baryon transitions between ground state baryons was subject to the octet rule due to the simple Fierz property of the nonleptonic current-current product. This discovery is sometimes referred to as the Pati-Woo theorem [39] even though the discovery of Pati and Woo was predated by the paper [40].

4 Counting Spin Observables

When setting up a problem involving the spin of particles it is always instructive to first denumerate the complexity of the problem and count the number of independent

Table 2: Independent components of the single spin density matrix

spin	rate	real	imaginary	sum
J	trace	$J(2J + 3)$	$J(2J + 1)$	$(2J + 1)^2$
$J = 1/2$	1	2	1	4
$J = 1$	1	5	3	9
$J = 3/2$	1	9	6	16

structures of the problem. A particularly efficient and physical way to do so is to count the number of independent elements of the spin density matrices involved in the process.

The single spin density matrix $\rho_{\lambda\lambda'}$ is a $(2J+1)(2J+1)$ hermitian matrix ($\rho_{\lambda\lambda'} = \rho_{\lambda'\lambda}^*$). It thus has $(2J+1)^2$ independent components of which $(J+1)(2J+1)$ are real and $J(2J+1)$ are imaginary. The rate is represented by the trace of the density matrix. In Table 2 we list the corresponding degrees of freedom for the first few spin cases $J = 1/2, 1, 3/2$. The density matrix is also frequently represented in terms of its angular momentum content. For the three cases listed in Table 2 the angular momentum content is given by $1/2 \otimes 1/2 = 0 \oplus 1$, $1 \otimes 1 = 0 \oplus 1 \oplus 2$ and $3/2 \otimes 3/2 = 0 \oplus 1 \oplus 2 \oplus 3$ where the one-dimensional representation “0” is equivalent to the trace or rate. It is clear that one obtains the correct respective number of spin degrees of freedom $(2J+1)^2$ in Table 2 when adding up the dimensions of the angular momentum spaces appearing in the decomposition $J \otimes J = 0 \oplus \dots \oplus 2J$.

In the spin 1/2 case the four spin degrees of freedom are the rate, the two real components and the imaginary component of the spin 1/2 density matrix. The unnormalized density matrix ρ is usually written as

$$\begin{aligned}
 \rho_{\lambda\lambda'} &= \begin{pmatrix} h_{+1/2} h_{1/2}^* & h_{+1/2} h_{-1/2}^* \\ h_{-1/2} h_{1/2}^* & h_{-1/2} h_{-1/2}^* \end{pmatrix} \\
 &= \frac{1}{2} (\sigma \cdot \mathbb{1} + \vec{\xi} \cdot \vec{\sigma}).
 \end{aligned} \tag{20}$$

In the helicity basis the four spin degrees of freedom are labelled by

$$\sigma : \text{rate},$$

$$\begin{aligned}
\xi_x/\sigma &: \text{“perpendicular” polarization } P^\perp, \\
\xi_y/\sigma &: \text{“normal” polarization } P^N, \\
\xi_z/\sigma &: \text{“longitudinal” polarization } P^l.
\end{aligned}
\tag{21}$$

The y -component P^N can be seen to be a T -odd measure since one needs a vector product to construct the normal to a given plane. For example, in μ -decay P^N is determined by the expectation value $\langle \vec{\sigma}_e \cdot (\vec{\sigma}_\mu \times \vec{p}_e) \rangle$ which is a T -odd measure. In the context of this review P^N obtains contributions only from the imaginary parts of one-loop diagrams. For all processes listed in Table 1 in Sect. 1 the one-loop diagrams are real and thus $P^N = 0$ in these processes. This is different in $e^+e^- \rightarrow q\bar{q}g$ where the one-loop diagrams possess imaginary parts and where one therefore has $P^N \neq 0$ (see e.g. [14, 41]).

Returning to Table 2 we shall see that not all $(2J+1)^2$ spin degrees of freedom are accessible (angular momentum conservation) or measurable (parity) in general.

In the following we will be concerned with double spin density matrices. Their spin degrees of freedom are given by the products of the single spin degrees of freedom. For the cases discussed in this review the double density matrix is a sparsely populated matrix, due to angular momentum conservation and the absence of imaginary parts from loop contributions. Take, for example, the double spin density matrix of the decay $t(\uparrow) \rightarrow X_b + W^+(\uparrow)$. On naive counting one would expect $N = (1(\text{trace}) + 20(\text{real}) + 15(\text{imaginary}))$ spin degrees of freedom. This number is considerably reduced by considering the following two facts.

1. The one-loop amplitude does not possess an imaginary (absorptive) part. This can be seen by taking a look at the one-loop vertex corrections for the transitions discussed in Table 1. The vertex correction does not admit of real on-shell intermediate states, i.e. it does not have an absorptive part. The 15 imaginary components of the double density matrix are zero.
2. Angular momentum conservation. In the rest frame of the top the decay into X_b and W^+ is back-to-back and thus anti-collinear. Since one is summing over the helicities of the X_b one has $\lambda_{X_b} = \lambda'_{X_b}$ and thus $\lambda_t - \lambda_W = \lambda'_t - \lambda'_W$ (see Fig. 3). Taking this constraint into consideration one remains with six diagonal and two non-diagonal double spin density matrix elements (see Table 3) where one refers to diagonal and non-diagonal elements when $(\lambda_t, \lambda_W) = (\lambda'_t, \lambda'_W)$ and $(\lambda_t, \lambda_W) \neq (\lambda'_t, \lambda'_W)$, respectively. One has non-diagonal transitions for the two cases $\lambda_t - \lambda_W = \pm 1/2$. Concerning the non-diagonal density matrix elements it is easy to see from the master formula (26) to be discussed in Sect. 5 that they generate azimuthal dependences in angular decay distributions.

We shall now go through the exercise and count the spin degrees of freedom by a different method, namely by counting the number of covariants of the process. We emphasize that counting spin degrees of freedom via density matrix elements is generally safer than counting the number of independent covariants because there exist nontrivial identities between covariants in $D = 4$ dimensions. The decay $t(\uparrow) \rightarrow X_b + W^+(\uparrow)$ will illustrate this point.

Consider the expansion of the spin dependent hadron tensor of the process into covariants constructed from the metric tensor, the Levi–Civita tensor, the independent momenta of the process and the spin four–vector of the top. One has

$$\begin{aligned}
H^{\mu\nu} &= (-g^{\mu\nu} H_1 + p_t^\mu p_t^\nu H_2 - i\epsilon^{\mu\nu\rho\sigma} p_{t,\rho} q_\sigma H_3) \\
&- (q \cdot s_t)(-g^{\mu\nu} G_1 + p_t^\mu p_t^\nu G_2 - i\epsilon^{\mu\nu\rho\sigma} p_{t,\rho} q_\sigma G_3) \\
&+ (s_t^\mu p_t^\nu + s_t^\nu p_t^\mu) G_6 + i\epsilon^{\mu\nu\rho\sigma} p_{t\rho} s_{t\sigma} G_8 + i\epsilon^{\mu\nu\rho\sigma} q_\rho s_{t\sigma} G_9.
\end{aligned} \tag{22}$$

There are nine covariants and associated with it nine invariants which obviously does not agree with the number eight counted before using helicity counting. The discrepancy arises because there exist a nontrivial four–dimensional identity between three of the nine covariants which reads

$$q \cdot s_t \epsilon^{\mu\nu\rho\sigma} p_{t,\rho} q_\sigma - q^2 \epsilon^{\mu\nu\rho\sigma} p_{t,\rho} s_{t\sigma} + q \cdot p_t \epsilon^{\mu\nu\rho\sigma} q_\rho s_{t,\sigma} = 0. \tag{23}$$

This identity can be derived using the Schouten identity which reads

$$T_{\mu[\mu_1\mu_2\mu_3\mu_4\mu_5]} = 0, \tag{24}$$

where the symbol “[...]” denotes antisymmetrization and where

$$T_{\mu[\mu_1\mu_2\mu_3\mu_4\mu_5]} = g_{\mu\mu_1} \epsilon_{\mu_2\mu_3\mu_4\mu_5} + \text{cycl.}(\mu_1, \mu_2, \mu_3, \mu_4, \mu_5). \tag{25}$$

The Schouten identity is just the statement that it is impossible to place four index values in an antisymmetric fifth rank tensor, or in the language of Young Tableaux, that a Young Tableau with five vertical boxes is identically zero in four dimensions.

This illustration is not only of academic interest but has numerical implications since one can get into a terrible mess numerically if one works with a redundant set of covariants and tries to do matrix inversions involving the overcounted set of degrees of freedom. Although the Schouten identity seems rather obvious nowadays there have been examples in the literature where Schouten–type of identities have been overlooked.

Table 3: Non-vanishing double density matrix elements in $t(\uparrow) \rightarrow X_b + W^+(\uparrow)$

λ_t	λ_W	$\lambda_t - \lambda_W$
1/2	1	-1/2
1/2	0	1/2
1/2	-1	3/2
-1/2	1	-3/2
-1/2	0	-1/2
-1/2	-1	1/2

We conclude this section by enumerating the number of spin degrees of freedom in the various decay processes discussed in this review. The processes are listed in Table 4 together with the number of spin degrees of freedom. The corresponding references to the papers in which these decays were treated can be found in Table 1. In this list we have taken into account that the decay $D^* \rightarrow \pi(\gamma)$ is parity conserving. In parantheses we list the number of T -odd observables for each process which are zero due to the absence of imaginary contributions in the one-loop vertex correction.

5 Angular Decay Distributions

It should be clear that one needs to do polarization measurements in order to disentangle the full structure of particle interactions. Polarization measurements are particularly simple when the particle whose polarization one wants to measure decays. The angular decay distribution of the decay products reveals information on the state of polarization of the decaying particle. The information contained in the angular decay distribution is maximal when the particle decay is weak. The fact that the angular decay distribution reveals information on the polarization of the decaying particle is sometimes referred to as that the particle decay is self-analyzing.

There are principally two ways to obtain angular decay distributions which we will refer to as the non-covariant and the covariant methods. In the non-covariant method one makes use of rotation matrices whereas in the covariant method one evaluates scalar prod-

Table 4: Number of measurable double density matrix elements for the processes listed in Table 1

process	spin degrees of freedom
$t(\uparrow) \longrightarrow b + W^+(\uparrow)$	$N = 1 + 7 (+2)$
$t(\uparrow) \longrightarrow b + H^+$	$N = 1 + 1$
$B \longrightarrow X_c + D_s$	$N = 1$
$B \longrightarrow X_c + D_s^*(\uparrow)$	$N = 1 + 1$
$\Lambda_b(\uparrow) \longrightarrow X_c + D_s$	$N = 1 + 1$
$\Lambda_b(\uparrow) \longrightarrow X_c + D_s^*(\uparrow)$	$N = 1 + 4 (+1)$
$l(\uparrow) \longrightarrow l'(\uparrow) + \nu_l + \nu_{l'}$	$N = 1 + 4 (+1)$

ucts of four-vectors involving momenta and spin four-vectors in given reference frames. We shall discuss one example each of the two methods.

As an example for the non-covariant method we write down the angular decay distribution of polarized top decay $t(\uparrow) \rightarrow b + W^+$ followed by $W^+ \rightarrow l^+ + \nu_l$. The angular decay distribution can be obtained from the master formula

$$W(\theta_P, \theta, \phi) \propto \sum_{\lambda_W - \lambda'_W = \lambda_t - \lambda'_t} e^{i(\lambda_W - \lambda'_W)\phi} d_{\lambda_W 1}^1(\theta) d_{\lambda'_W 1}^1(\theta) H_{\lambda_W \lambda'_W}^{\lambda_t \lambda'_t} \rho_{\lambda_t \lambda'_t}(\theta_P), \quad (26)$$

where $\rho_{\lambda_t \lambda'_t}(\theta_P)$ is the density matrix of the top quark which reads

$$\rho_{\lambda_t \lambda'_t}(\theta_P) = \frac{1}{2} \begin{pmatrix} 1 + P \cos \theta_P & P \sin \theta_P \\ P \sin \theta_P & 1 - P \cos \theta_P \end{pmatrix}. \quad (27)$$

P is the magnitude of the polarization of the top quark. The $H_{\lambda_W \lambda'_W}^{\lambda_t \lambda'_t}$ are helicity matrix elements of the hadronic structure function $H_{\mu\nu}$. The sum in (26) extends over all values of $\lambda_W, \lambda'_W, \lambda_t$ and λ'_t compatible with the constraint $\lambda_W - \lambda'_W = \lambda_t - \lambda'_t$. The second lower index in the small Wigner $d(\theta)$ -function $d_{\lambda_W 1}^1$ is fixed at $m = 1$ for zero mass leptons because the total m -quantum number of the lepton pair along the l^+ direction is $m = 1$. Because there exist different conventions for Wigner's d -functions we explicate the requisite components that enter (26): $d_{11}^1 = (1 + \cos \theta)/2$, $d_{01}^1 = \sin \theta/\sqrt{2}$ and $d_{-11}^1 = (1 - \cos \theta)/2$. The fact that one has to specify the phase convention of the Wigner's

d -functions points to one of the weaknesses of the non-covariant method to obtain the correct angular decay distributions: one has to use one set of consistent phase conventions to obtain the correct signs for the angular factors. For someone not so familiar with the angular momentum apparatus this is not always simple. For the polar angle dependencies the correctness of a sign can always be checked by using physics arguments. This is more difficult for the azimuthal signs.

Including the appropriate normalization factor the four-fold decay distribution is given by [4, 6]

$$\begin{aligned} \frac{d\Gamma}{dq_0 d \cos \theta_P d \cos \theta d \phi} &= \frac{1}{4\pi} \frac{G_F |V_{tb}|^2 m_W^2}{\sqrt{2} \pi} |\vec{q}| \left\{ \right. \\ &+ \frac{3}{8} (H_U + P \cos \theta_p H_{UP}) (1 + \cos^2 \theta) \\ &+ \frac{3}{4} (H_L + P \cos \theta_p H_{LP}) \sin^2 \theta + \frac{3}{4} (H_F + P \cos \theta_p H_{FP}) \cos \theta \\ &\left. + \frac{3}{2\sqrt{2}} P \sin \theta_p H_{IP} \sin 2\theta \cos \phi + \frac{3}{\sqrt{2}} P \sin \theta_p H_{AP} \sin \theta \cos \phi \right\}, \quad (28) \end{aligned}$$

where the helicity structure functions H_U, H_L etc. are linear combinations of the helicity matrix elements $H_{\lambda_t \lambda'_t \lambda_W \lambda'_W}$. We have taken the freedom to normalize the differential rate such that one obtains the total $t \rightarrow b + W^+$ rate upon integration *and not* the total rate multiplied by the branching ratio of the respective W^+ decay channel.

The polar angles θ_P and θ , and the azimuthal angle ϕ that arise in the full cascade-type description of the two-stage decay process $t(\uparrow) \rightarrow W^+(\rightarrow l^+ + \nu_l) + X_b$ are defined in Fig. 4. For better visibility we have oriented the lepton plane with a negative azimuthal angle relative to the hadron plane. For the hadronic decays of the W into a pair of light quarks one has to replace (l^+, ν_l) by (\bar{q}, q) in Fig. 4. We mention that we have checked the signs of the angular decay distribution (28) using covariant techniques.

At first sight it seems rather strange that the angular analysis is done in two different coordinate systems, namely the top quark rest system and the W rest system. This runs counter to common wisdom that invariants should always be evaluated in one reference system. Some insight into the problem may be gained by using the orthonormality and completeness relation of polarization vectors to rewrite the contraction of the hadron and lepton tensors in a form which exhibits the correctness of using two different reference systems for the cascade decay. The orthonormality and completeness relation read

$$\text{Orthonormality:} \quad g_{\mu\nu} \epsilon^{*\mu}(m) \epsilon^\nu(m') = g_{mm'} \quad m, m' = S, \pm, 0, \quad (29)$$

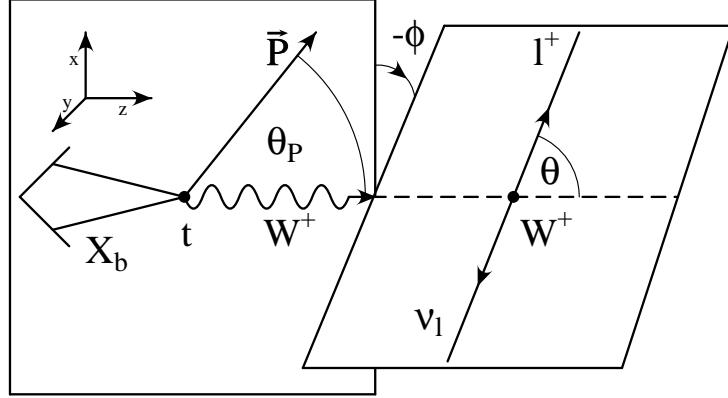


Figure 4: Definition of the angles θ_P , θ and ϕ in the cascade decay $t(\uparrow) \rightarrow X_b + W^+$ and $W^+ \rightarrow l^+ + \nu_l$

$$\text{Completeness:} \quad \sum_{m,m'=S,\pm,0} \epsilon^\mu(m) \epsilon^{*\nu}(m') g_{mm'} = g^{\mu\nu} \quad \mu, \nu = 0, 1, 2, 3, \quad (30)$$

where $g_{mm'} = \text{diag}(+, -, -, -)$, $(m, m' = S, \pm, 0)$ and $g^{\mu\nu} = \text{diag}(+, -, -, -)$, $(\mu, \nu = 0, 1, 2, 3)$. The scalar or time component of the polarization four-vector is denoted by S . On using the completeness relation one then has

$$\begin{aligned} L^{\mu\nu} H_{\mu\nu} &= L_{\mu'\nu'} g^{\mu'\mu} g^{\nu'\nu} H_{\mu\nu} = L_{\mu'\nu'} \epsilon^{\mu'}(m) \epsilon^{*\mu}(m') g_{mm'} \epsilon^{*\nu'}(n) \epsilon^\nu(n') g_{nn'} H_{\mu\nu} \\ &= (L_{\mu'\nu'} \epsilon^{\mu'}(m) \epsilon^{*\nu'}(n)) (H_{\mu\nu} \epsilon^{*\mu}(m') \epsilon^\nu(n')) g_{mm'} g_{nn'}. \end{aligned} \quad (31)$$

The point is that the two Lorentz contractions appearing on the second line of (31) can be evaluated in two different Lorentz frames. The leptonic invariant $L_{\mu'\nu'} \epsilon^{\mu'}(m) \epsilon^{*\nu'}(n)$ can be evaluated in the $(l\nu)$ CM frame (or in the W^+ rest frame) while the hadronic invariant $H_{\mu\nu} \epsilon^{*\mu}(m') \epsilon^\nu(n')$ can be evaluated in the rest frame of the top quark. Another advantage of this method is that one can easily incorporate lepton mass effects as is mandatory for $b \rightarrow c$ or the rare $b \rightarrow s$ transitions if the charged lepton or leptons in the final state are τ leptons. This technique was used to derive angular decay distributions including leptonic polarization effects for semileptonic and rare bottom meson decays in [42] and [43]. Note also that the correct phase choice for the polarization vectors is no longer crucial since the polarization vectors always appear as squares in the orthonormality and completeness relations.

As an example of the covariant method we discuss the angular decay distribution of polarized μ decay into a polarized e . From helicity counting as described in Sect. 4 one knows that there are altogether five spin-dependent structure functions and one spin-independent structure function describing the leptonic decay of a polarized muon into a polarized electron. We thus define a spin-dependent differential rate in terms of six invariant structure functions A_i . Accordingly one has [3]

$$\begin{aligned} \frac{d\Gamma}{dx d\cos\theta_P} &= A_1 + \frac{1}{m_\mu} A_2(p_e \cdot s_\mu) + \frac{1}{m_\mu} A_3(p_\mu \cdot s_e) + \frac{1}{m_\mu^2} A_4(p_e \cdot s_\mu)(p_\mu \cdot s_e) \\ &+ A_5(s_\mu \cdot s_e) + \frac{1}{m_\mu^2} A_6 \epsilon_{\alpha\beta\gamma\delta} p_\mu^\alpha p_e^\beta s_\mu^\gamma s_e^\delta. \end{aligned} \quad (32)$$

Eq. (32) will be evaluated in the rest system of the muon where $p_\mu = (m_\mu; 0, 0, 0)$ and $p_e = (E_e; 0, 0, |\vec{p}_e|) = (m_\mu/2)(x; 0, 0, x\beta)$. The velocity of the electron is denoted by $\beta = \sqrt{1 - 4y^2/x^2}$ where $y = m_e/m_\mu$ and $x = 2E_e/m_\mu$ denotes the scaled energy of the electron. In the rest frame of the μ^- the polarization four-vectors of the μ^- and e^- are given by

$$s_\mu^\alpha = (0; \vec{\zeta}_\mu), \quad (33)$$

$$s_e^\alpha = \left(\frac{\vec{n}_e \cdot \vec{p}_e}{m_e}; \vec{n}_e + \frac{\vec{n}_e \cdot \vec{p}_e}{m_e(E_e + m_e)} \vec{p}_e \right), \quad (34)$$

where the polarization three-vector $\vec{\zeta}_\mu$ of the μ^- and the quantization axis \vec{n}_e of the spin of the e^- in their respective rest frames read (see Fig. 5)

$$\vec{\zeta}_\mu = (\sin\theta_P, 0, \cos\theta_P) \quad (35)$$

and

$$\vec{n}_e = (\sin\theta \cos\chi, \sin\theta \sin\chi, \cos\theta). \quad (36)$$

Eq. (35) holds for 100% polarized muons. For partially polarized muons with magnitude of polarization P the representation (35) has to be multiplied by P such that $\vec{P}_\mu = P\vec{\zeta}_\mu$.

The scalar products in (32) can then be evaluated with the result

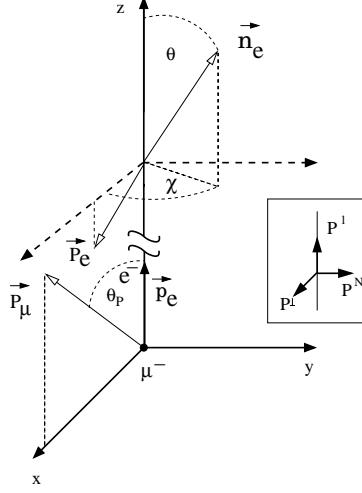


Figure 5: Definition of the angles θ_P , θ and χ in polarized muon decay

$$\begin{aligned}
p_e \cdot s_\mu &= -\frac{m_\mu}{2} x \beta P \cos \theta_P, \\
p_\mu \cdot s_e &= \frac{m_\mu}{2y} x \beta \cos \theta, \\
s_\mu \cdot s_e &= -P \sin \theta_P \sin \theta \cos \chi, \\
\epsilon_{\alpha\beta\gamma\delta} p_\mu^\alpha p_e^\beta s_\mu^\gamma s_e^\delta &= \frac{m_\mu^2}{2} x \beta P \sin \theta_P \sin \theta \sin \chi.
\end{aligned} \tag{37}$$

Including the correct normalization one finally arrives at the angular decay distribution [3]

$$\begin{aligned}
\frac{d\Gamma}{dx d\cos \theta_P} &= \beta x \Gamma_0 (G_1 + G_2 P \cos \theta_P + G_3 \cos \theta + G_4 P \cos \theta_P \cos \theta \\
&+ G_5 P \sin \theta_P \sin \theta \cos \chi + G_6 P \sin \theta_P \sin \theta \sin \chi),
\end{aligned} \tag{38}$$

where the relation between the invariant structure functions A_i and the frame-dependent spectrum functions G_i can be found in [3]. G_1 is the unpolarized spectrum function, G_2 and G_3 are single spin polarized spectrum functions referring to the spins of the μ^- and e^- , resp., and G_4 , G_5 and G_6 describe spin-spin correlations between the spin vectors of the muon and electron. G_6 represents a so-called T -odd observable. This is

evident when rewriting the angular factor multiplying G_6 in (38) in triple-product form, i.e. $\sin \theta_P \sin \theta \sin \chi = |\vec{p}_e|^{-1} \vec{p}_e \cdot (\vec{\zeta}_\mu \times \vec{n}_e)$. As stated before G_6 is identically zero in the Standard Model since, on the one hand, the weak coupling constant G_F is real and, on the other hand, the loop contributions do not generate imaginary parts. In the terminology of Sect. 4 G_1-G_4 are diagonal structure functions, while the azimuthally dependent structure functions G_5 and G_6 are non-diagonal. As mentioned before, the structure function G_5 is proportional to the electron mass and therefore vanishes for $m_e \rightarrow 0$. Naturally, the angular decay distribution (38) can also be derived in the helicity formalism.

In the two examples discussed in this section we chose to orient the z -axis along the three-momentum of one of the particles. In this case one says that the angular analysis is done in the helicity system. Of course, other choices of the orientation of the z -axis are possible. A popular choice is the transversity system where the z -axis is normal to a given plane spanned by the momenta of the decay products. A more detailed discussion of the choice of frames can be found in [42] where the angular decay distribution in the semileptonic decays $B \rightarrow (D, D^*) + l + \nu$ including lepton mass effects was investigated. We mention that the transversity system is the preferred choice when discussing the CP properties of the final state [44].

6 One-Loop Amplitude

We present our results in terms of the three vector current amplitudes F_i^V ($i = 1, 2, 3$) and the three axial vector current amplitudes F_i^A ($i = 1, 2, 3$) defined by ($J_\mu^V = \bar{q}_b \gamma_\mu q_t$, $J_\mu^A = \bar{q}_b \gamma_\mu \gamma_5 q_t$)

$$\langle b(p_b) | J_\mu^V | t(p_t) \rangle = \bar{u}_b(p_b) \left\{ \gamma_\mu F_1^V + p_{t,\mu} F_2^V + p_{b,\mu} F_3^V \right\} u_t(p_t), \quad (39a)$$

$$\langle b(p_b) | J_\mu^A | t(p_t) \rangle = \bar{u}_b(p_b) \left\{ \gamma_\mu F_1^A + p_{t,\mu} F_2^A + p_{b,\mu} F_3^A \right\} \gamma_5 u_t(p_t). \quad (39b)$$

In this Section we choose to label the current transition according to the transition $t \rightarrow b$ as in [6]. As emphasized before, up to the colour factor identical expressions are obtained for the $\mu \rightarrow e$ transition if the leptonic four-fermion interaction is written in the charge retention form. For the form factors one obtains [6]

$$F_1^V = 1 + \frac{\alpha_s}{4\pi} C_F \left\{ - \frac{m_t^2 + m_b^2 - q^2}{m_t^2 \sqrt{\lambda}} \left[2 \text{Li}_2(1 - w_1^2) - 2 \text{Li}_2\left(1 - \frac{w_1}{w_\mu}\right) \right] \right\} \quad (40a)$$

$$\begin{aligned}
& + \frac{1}{2} \ln \left(\frac{\Lambda^4}{m_b^2 m_t^2} \right) \ln(w_1 w_\mu) + \ln \left(\frac{w_1^3}{w_\mu} \right) \ln \left(\frac{w_\mu (1 - w_1^2)}{w_\mu - w_1} \right) \Big] - \ln \left(\frac{\Lambda^4}{m_b^2 m_t^2} \right) \\
& - \frac{m_t^2 - m_b^2}{2q^2} \ln \left(\frac{m_b^2}{m_t^2} \right) - 4 + \ln(w_1 w_\mu) \left(\frac{m_t^2 \sqrt{\lambda}}{2q^2} - \frac{(m_t + m_b)^2 - q^2}{m_t^2 \sqrt{\lambda}} \right) \Big\}, \\
F_2^V &= \frac{\alpha_s}{4\pi} C_F \frac{m_t - m_b}{q^2} \left\{ 2 - \left(\frac{m_t + 2m_b}{m_t - m_b} - \frac{m_t^2 - m_b^2}{q^2} \right) \ln \left(\frac{m_b^2}{m_t^2} \right) \right. \\
& \left. - \left(\frac{m_t^2 \sqrt{\lambda}}{q^2} - \frac{m_b}{m_t - m_b} \frac{q^2 + (m_t - m_b)(3m_t + m_b)}{m_t^2 \sqrt{\lambda}} \right) \ln(w_1 w_\mu) \right\}, \\
F_3^V &= F_3^V(m_t, m_b) = F_2^V(m_b, m_t), \tag{40c}
\end{aligned}$$

where we have denoted the scaled (small) gluon mass by $\Lambda = m_g/m_t$. We define $\lambda = 1 + x^4 + y^4 - 2x^2 y^2 - 2x^2 - 2y^2$ ($x = q^2/m_t^2$, $y = m_b/m_t$) and use the abbreviations

$$w_1 = \frac{x}{y} \frac{1 - x^2 + y^2 - \sqrt{\lambda}}{1 + x^2 - y^2 + \sqrt{\lambda}}, \quad w_\mu = \frac{x}{y} \frac{1 - x^2 + y^2 - \sqrt{\lambda}}{1 + x^2 - y^2 - \sqrt{\lambda}}. \tag{41}$$

The axial vector amplitudes F_i^A can be obtained from the vector amplitudes by the replacement $m_t \rightarrow -m_t$, i.e. one has $F_i^A(m_t) = F_i^V(-m_t)$ ($i = 1, 2, 3$). Our one-loop amplitudes are linearly related to the one-loop amplitudes given in [45] after correcting for a typo in [45] (see also [46]).

Note that the infrared singularities proportional to $\ln \Lambda$ and the would-be mass singularities (also called collinear singularities) proportional to $\ln m_b$ all reside in the Born term form factors F_1^V and F_1^A . They are eventually cancelled by the corresponding singularities in the tree graph contribution. A look at the arguments of the log and dilog functions in 40a shows that the one-loop contribution is purely real as remarked on earlier.

In the case of the electroweak radiative corrections to $t \rightarrow b + W^+$ there are altogether 18 different vertex correction diagrams in the Feynman-'t Hooft gauge [7] as compared to the one vertex correction diagram in the QCD and the μ -decay cases discussed in this section. In addition to the massive one-loop three-point functions one has to calculate the many massive one-loop two-point functions needed in the renormalization program. We have recalculated all one-loop contributions analytically and have checked them analytically and numerically with the help of a XLOOPS/GiNaC package that automatically calculates one-loop two-point and three-point functions [47]. Our one-loop results agree with the results of [48]. The results are too lengthy to be reproduced here in analytical form. The full analytical results will be given in a forthcoming publication [49].

7 Tree-Graph Contribution

As emphasized earlier on, the *NLO* tree graph contributions for the QED and QCD cases are identical up to *NLO* except for a trivial colour factor in the case of QCD. Differences set in only at *NNLO* where three-gluon coupling contributions come in. We choose to present and discuss the *NLO* tree graph contributions in the QED radiative corrections to leptonic μ -decay as written down in [3].

We begin with the Born term contribution. This is an exercise that everyone has probably gone through before in the unpolarized case. The point that not everyone is familiar with is that it is very simple to include the spin of fermions at the Born term level. All that is needed is the substitution $p \rightarrow \bar{p}$ for the fermion's momenta where the notation \bar{p} is explained in the following. The $p \rightarrow \bar{p}$ rule is best explained by looking at the trace expression of the charge-side tensor which reads

$$C_{Born}^{\alpha\beta} = \frac{1}{4} \text{Tr} \left\{ (\not{p}_e + m_e) (\mathbb{1} + \gamma_5 \not{s}_e) \gamma^\alpha (\mathbb{1} - \gamma_5) (\not{p}_\mu + m_\mu) (\mathbb{1} + \gamma_5 \not{s}_\mu) \gamma^\beta (\mathbb{1} - \gamma_5) \right\}. \quad (42)$$

The dependence on the polarization four-vectors of the μ^- and e^- has been retained in (42).

Since only even-numbered γ -matrix strings survive between the two $(\mathbb{1} - \gamma_5)$ -factors in (42) one can compactly write the result of the trace evaluation as

$$C_{Born}^{\alpha\beta} = 2(\bar{p}_\mu^\beta \bar{p}_e^\alpha + \bar{p}_\mu^\alpha \bar{p}_e^\beta - g^{\alpha\beta} \bar{p}_\mu \cdot \bar{p}_e + i\epsilon^{\alpha\beta\gamma\delta} \bar{p}_{e,\gamma} \bar{p}_{\mu,\delta}), \quad (43)$$

where

$$\bar{p}_\mu^\alpha = p_\mu^\alpha - m_\mu s_\mu^\alpha, \quad (44a)$$

$$\bar{p}_e^\alpha = p_e^\alpha - m_e s_e^\alpha, \quad (44b)$$

and where s_μ^α and s_e^α are the polarization four-vectors of the μ^- and e^- .

In the QED case one has the simplifying feature that the contribution of the last term antisymmetric in $(\alpha\beta)$ can be dropped. The reason is that the dependence on the momentum directions of the $\bar{\nu}_e$ - and ν_μ -neutrinos is completely integrated out in the differential rate. Thus the neutrino-side of the interaction can only depend on the spatial piece of the second rank tensor build from the momentum transfer to the neutrinos (the neutrinos are treated as massless) which is symmetric in $(\alpha\beta)$. Upon contraction with the charge-side tensor the antisymmetric piece drops out.

Unfortunately the $p \rightarrow \bar{p}$ trick no longer works at NLO order. But still, by using the \bar{p} -notation, the result can be presented in a very compact form. The result for the NLO $\mu \rightarrow e$ tree graph contribution reads

$$\begin{aligned}
C^{\alpha\beta} &= \sum_{\gamma\text{-spin}} \mathcal{M}^\alpha \mathcal{M}^{\beta\dagger} = \frac{e^2}{2} \left\{ \left(\frac{k \cdot \bar{p}_e - m_e^2}{k \cdot p_e} + \frac{p_\mu \cdot \bar{p}_e}{k \cdot p_\mu} \right) \frac{k^\alpha \bar{p}_\mu^\beta + k^\beta \bar{p}_\mu^\alpha - k \cdot \bar{p}_\mu g^{\alpha\beta}}{k \cdot p_e} \right. \\
&+ \left(\frac{k \cdot \bar{p}_\mu + m_\mu^2}{k \cdot p_\mu} - \frac{p_e \cdot \bar{p}_\mu}{k \cdot p_e} \right) \frac{k^\alpha \bar{p}_e^\beta + k^\beta \bar{p}_e^\alpha - k \cdot \bar{p}_e g^{\alpha\beta}}{k \cdot p_\mu} \\
&+ (k \cdot \bar{p}_\mu) \frac{p_e^\alpha \bar{p}_e^\beta + p_e^\beta \bar{p}_e^\alpha - m_e^2 g^{\alpha\beta}}{(k \cdot p_e)(k \cdot p_\mu)} - (k \cdot \bar{p}_e) \frac{p_\mu^\alpha \bar{p}_\mu^\beta + p_\mu^\beta \bar{p}_\mu^\alpha - m_\mu^2 g^{\alpha\beta}}{(k \cdot p_e)(k \cdot p_\mu)} \\
&+ \left. (k \cdot \bar{p}_e) \frac{p_e^\alpha \bar{p}_\mu^\beta + p_e^\beta \bar{p}_\mu^\alpha - p_e \cdot \bar{p}_\mu g^{\alpha\beta}}{(k \cdot p_e)^2} - (k \cdot \bar{p}_\mu) \frac{p_\mu^\alpha \bar{p}_e^\beta + p_\mu^\beta \bar{p}_e^\alpha - p_\mu \cdot \bar{p}_e g^{\alpha\beta}}{(k \cdot p_\mu)^2} \right\} \\
&- \frac{e^2}{2} \left(\frac{m_\mu^2}{(k \cdot p_\mu)^2} + \frac{m_e^2}{(k \cdot p_e)^2} - \frac{2p_e \cdot p_\mu}{(k \cdot p_e)(k \cdot p_\mu)} \right) (\bar{p}_e^\alpha \bar{p}_\mu^\beta + \bar{p}_e^\beta \bar{p}_\mu^\alpha - \bar{p}_e \cdot \bar{p}_\mu g^{\alpha\beta}). \quad (45)
\end{aligned}$$

The momentum of the radiated photon is denoted by k . For the aforementioned reason we have dropped the contribution of antisymmetric terms. When the antisymmetric ϵ -tensor pieces are kept, and when one replaces $e \rightarrow g_s$ and $1 \rightarrow N_c C_F = 4$ to account for colour, one recovers the NLO QCD corrected hadronic tensor for the $t \rightarrow b$ transition listed in [6].

In the last line of (45) we have isolated the infrared singular piece of the charge-side tensor which is given by the usual soft photon factor multiplying the Born term contribution. Technically this is done by writing

$$C^{(\alpha)\alpha\beta} = \left(C^{(\alpha)\alpha\beta} - C^{(\alpha)\alpha\beta}(\text{softphoton}) \right) + C^{(\alpha)\alpha\beta}(\text{softphoton}). \quad (46)$$

The remaining part of the charge-side tensor in (45) is referred to as the hard photon contribution. It is infrared finite and can thus be integrated without a regulator photon mass.

Analytic phase space integrations without a regulator photon mass are much simpler. The regulator photon mass would introduce a new mass scale into the problem which, as emphasized before, would complicate the phase space integrations.

In the phase space integration over the photon momentum the infrared singular piece is regularized by introducing a (small) photon mass resulting in a logarithmic mass divergence in the photon mass. Since the integrand of the soft photon piece is much simpler

the phase space integration can be done analytically by carefully taking the appropriate mass zero limits in the integrations. The infrared divergence shows up as a logarithmic mass divergence in the photon mass. In addition, since the soft photon piece factors the Born term tensor, the Born term tensor can be pulled out of the phase space integrations. The resulting singular soft photon piece is therefore universal in the sense that it is the same for all spin structure functions, i.e. once the soft photon integration has been done for the rate the work is done. Eventually the infrared singular piece is cancelled by the corresponding singular piece in the one-loop contributions.

The approximation where only the soft photon (or gluon) piece is retained in the NLO tree-graph hadron tensor is called the soft photon (or gluon) approximation. From what has been said before it is clear that a NLO radiative correction calculation is much simplified in the soft photon (or gluon) approximation. In the next section we shall take a specific example, namely the process $e^+e^- \rightarrow t\bar{t}(g)$, to investigate the quality of the soft gluon approximation.

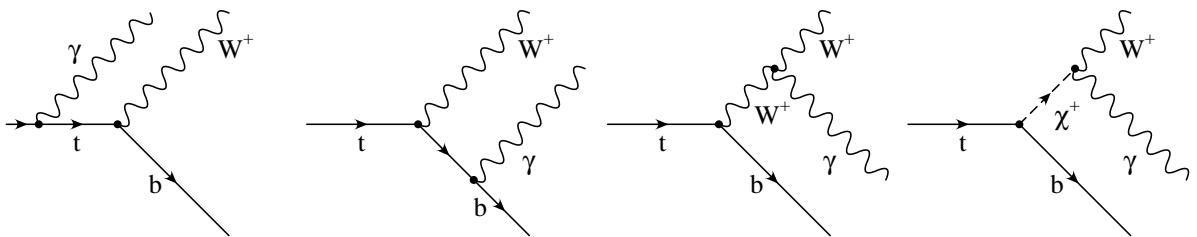


Figure 6: Tree-level Feynman graphs for $t \rightarrow b + W^+ + \gamma$ in the Feynman-'t Hooft gauge

It is interesting to note that the NLO hadronic tensor in the elektroweak corrections to the process $t \rightarrow b + W^+$ is only marginally more complicated than the corresponding tree graph contribution (45) although the number of contributing diagrams has doubled to four [7] (see Fig. 6). We do not list the finite piece of the hadronic tensor in this review but only write down the soft photon factor which multiplies the Born term tensor just as in (45). When discussing the decay $t \rightarrow b + W^+$ one has to of course include the antisymmetric ϵ -tensor piece in the Born term tensor. The soft photon contribution reads

$$\begin{aligned}
 -g^{\mu\nu} A_\mu^{(\text{s.ph.})} A_\nu^{(\text{s.ph.})} &= -e^2 \left(\frac{Q_t^2 m_t^2}{(p_t \cdot k)^2} + \frac{Q_b^2 m_b^2}{(p_b \cdot k)^2} + \frac{Q_W^2 m_W^2}{(q \cdot k)^2} \right. \\
 &\quad \left. - \frac{2Q_t Q_b p_t \cdot p_b}{(p_t \cdot k)(p_b \cdot k)} - \frac{2Q_t Q_W p_t \cdot q}{(p_t \cdot k)(q \cdot k)} + \frac{2Q_b Q_W p_b \cdot q}{(p_b \cdot k)(q \cdot k)} \right), \quad (47)
 \end{aligned}$$

where the soft photon amplitude is given by (see e.g. [51])

$$A^{(\text{s.ph.})\mu}\epsilon_\mu^* = e\left(\frac{Q_t p_t^\mu}{p_t \cdot k} - \frac{Q_b p_b^\mu}{p_b \cdot k} - \frac{Q_W q^\mu}{q \cdot k}\right)\epsilon_\mu^*. \quad (48)$$

$Q_t = 2/3$, $Q_b = -1/3$ and $Q_W = 1$ are the electric charges of the top quark, the bottom quark and the W -boson, resp., in units of the elementary charge e . Gauge invariance of the soft-photon amplitude is easily verified when replacing $\epsilon_\mu^* \rightarrow k_\mu$ in (48). It is then just a statement about charge conservation $Q_t - Q_b - Q_W = 0$. It is noteworthy that by setting $Q_t = Q_b = 1$ and $Q_W = 0$ in (47), one recovers the soft photon contribution in (45). In fact, the whole NLO electroweak tree-graph tensor in [7] reduces to the corresponding NLO QED tensor with the above charge replacements. In the same vein, the replacements $e \rightarrow g_s$ and $1 \rightarrow N_c C_F = 4$, to account for colour, and the replacements of the charge factors by $Q_t = Q_b = 1$ and $Q_W = 0$ will bring one from the electroweak case to the QCD case.

8 NLO Radiative Corrections to $e^+e^- \rightarrow t\bar{t}(g)$ in the Soft Gluon Approximation

In the soft gluon (or photon) approximation one keeps only the soft gluon (or photon) piece in the tree graph contribution but includes the full one-loop contribution. New structure is thus only generated by the one-loop contribution since the soft gluon piece has Born term structure. The structure contained in the hard part of the tree graph contribution is lost in the soft gluon approximation. A brief glance at the corresponding hard photon piece in (45) shows that it is considerably more difficult to do the analytic phase space integration for the hard part than for the soft photon piece. In particular, the integration of the hard photon piece has to be done separately for each density matrix element. Contrary to this, the integration of the soft photon piece has to be done only once since the Born term factor can be factored out of the integral. Technically, the soft gluon (or photon) approximation is much simpler than the full calculation if done analytically. Of course, if the calculation is done numerically, the integration of the hard gluon (or photon) part causes no additional problems. When the soft gluon (or photon) approximation is used this is done at the cost of losing interesting structure contained in the hard gluon (or photon) part.

In order to be able to judge the quality of the soft gluon approximation we have calculated the rate for $e^+e^- \rightarrow t\bar{t}(g)$ and have compared the results of the full calculation with the results of the soft gluon approximation using different cut-off values for the gluon

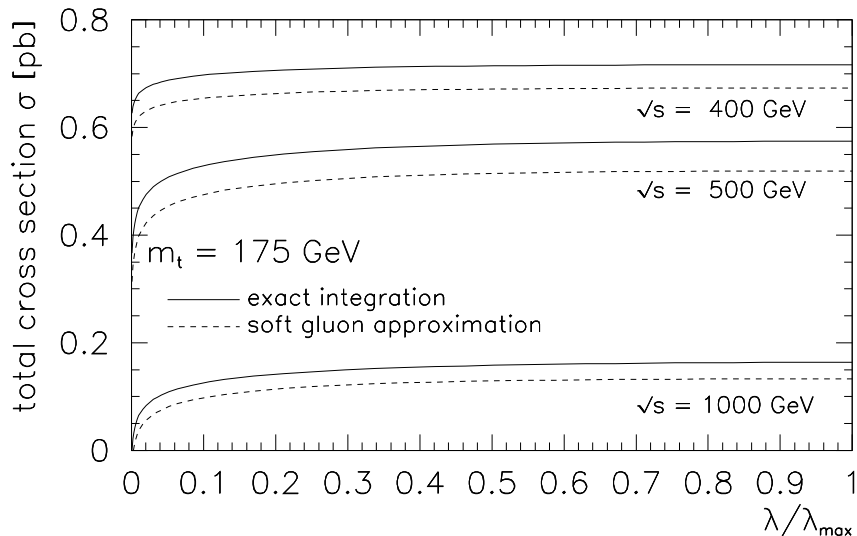


Figure 7: Total cross section for $e^+e^- \rightarrow t\bar{t}(g)$ as a function of the scaled gluon energy cut λ/λ_{max} for different c.m. energies. Full line: full calculation; dashed line: soft gluon approximation

energy [52]. Fig. 7 shows that the soft gluon result is below the full result for the whole range of cut-off values $\lambda = E_g/\sqrt{q^2}$ ($\lambda_{max} = 1 - 2m_t/\sqrt{q^2}$). For maximal cut-off values $\lambda = \lambda_{max}$ the soft gluon approximation is 3.4%, 5% and 11.5% below the full result at 400 GeV, 500 GeV and 1000 GeV, respectively. As emphasized above, much of the rate that is being missed by the soft gluon approximation has interesting structure.

9 Unpolarized Top Decay $t \rightarrow b + W^+$

We have already discussed various aspects of the decay $t \rightarrow b + W^+$ in previous sections. In this section we concentrate on unpolarized top decay. In particular, we want to discuss the mass dependence of the longitudinal piece of the W^+ boson the measurement of which could lead to an independent determination of the mass of the top quark.

The angular decay distribution for unpolarized top decay can be obtained by setting $P = 0$ in (28). The contribution of the three remaining structure functions H_L , H_U and H_F can be disentangled by a measurement of the shape of the lepton energy spectrum from top decay. Given enough data, one can hope to determine the longitudinal contribution with 1% accuracy [50].

At LO the mass dependence of the longitudinal contribution is given by $\Gamma_L/\Gamma = 1/(1+2(m_W/m_t)^2)$ which gives $\Gamma_L/\Gamma = 0.703$ using $m_t = 175$ GeV and $m_W = 80.419$ GeV. NLO corrections to the longitudinal contribution were calculated in [5, 6] (QCD) and in [7] (electroweak and finite width). Curiously enough the electroweak and finite width corrections tend to cancel each other in the structure functions. In Fig. 8 we show the top mass dependence of the ratio Γ_L/Γ . The Born term and the corrected curves are practically straight line curves. The horizontal displacement of the two curves is ≈ 3.5 GeV. One would thus make the corresponding mistake in the top mass determination from a measurement of Γ_L/Γ if the Born term curve were used instead of the corrected curve. If we take $m_t = 175$ GeV as central value, a 1% relative error on the measurement of Γ_L/Γ would allow one to determine the top quark mass with ≈ 3 GeV accuracy. Such a top mass measurement would be a welcome alternative to the usual invariant mass determination of the top quark mass since the Γ_L/Γ measurement is a completely independent measurement of the top quark mass.

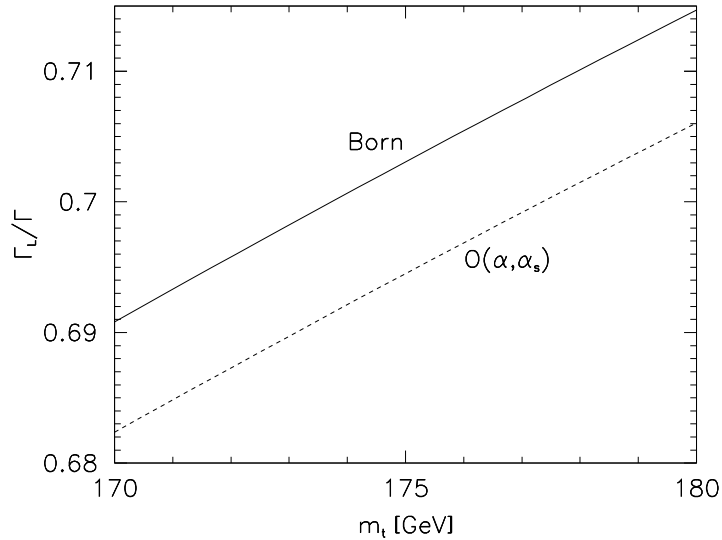


Figure 8: Top mass dependence of the ratio Γ_L/Γ (full line: LO, dashed line: corrections including QCD, electroweak (G_F -scheme), finite-width and ($m_b \neq 0$) Born term corrections)

10 The Decay $t(\uparrow) \rightarrow b + H^+$

Certain extensions of the minimal Standard Model with two Higgs–doublets (as e.g. the Minimal Supersymmetric Standard Model) contain charged Higgs bosons such that the decay $t(\uparrow) \rightarrow b + H^+$ would be possible if kinematically allowed. The Lagrangian for the decay reads

$$\mathcal{L} = \bar{\Psi}_b(x)(a + b\gamma_5)\Psi_t(x)\phi_{H^+}(x) + \text{h.c.} . \quad (49)$$

For the differential decay rate one obtains

$$\frac{d\Gamma}{d\cos\theta_P} = \frac{1}{2} \left(\Gamma + P\Gamma^P \cos\theta_P \right) = \frac{1}{2} \Gamma \left(1 + P\alpha_H \cos\theta_P \right), \quad (50)$$

where θ_P is the angle between the polarization vector of the top quark and the Higgs. The $\cos\theta_P$ –dependence in (50) is determined by the asymmetry parameter $\alpha_H = \Gamma/\Gamma_P$. At LO one obtains ($m_b = 0$)

$$\alpha_H = \frac{2ab}{a^2 + b^2}. \quad (51)$$

At this point we want to emphasize that one needs the polarization information contained in (50) to be able to determine the relative sign of the two coupling constants a and b . The rate is proportional to $(a^2 + b^2)$ and is therefore insensitive to the relative sign of the coupling constants.

We now specify to the so called model 2 where the coupling structure is expressed in terms of $\tan\beta = v_2/v_1$, and where v_1 and v_2 are the vacuum expectation values of the two neutral components of the two Higgs doublets. In model 2 the coupling constants are given by

$$a = \frac{g_w}{2\sqrt{2}m_W} V_{tb}(m_t \cot\beta + m_b \tan\beta), \quad (52)$$

$$b = \frac{g_w}{2\sqrt{2}m_W} V_{tb}(m_t \cot\beta - m_b \tan\beta). \quad (53)$$

The weak coupling factor g_w is related to the usual Fermi coupling constant G_F by $g_w = 2m_W\sqrt{2}\sqrt{G_F}$. In Fig. 9 we show a plot of the asymmetry parameter α_H as a function of the mass ratio m_H^+/m_t for a fixed value of $\tan\beta = 10$. The asymmetry parameter is large and negative over most of the range of mass ratios. The radiative corrections can be seen to be quite substantial.

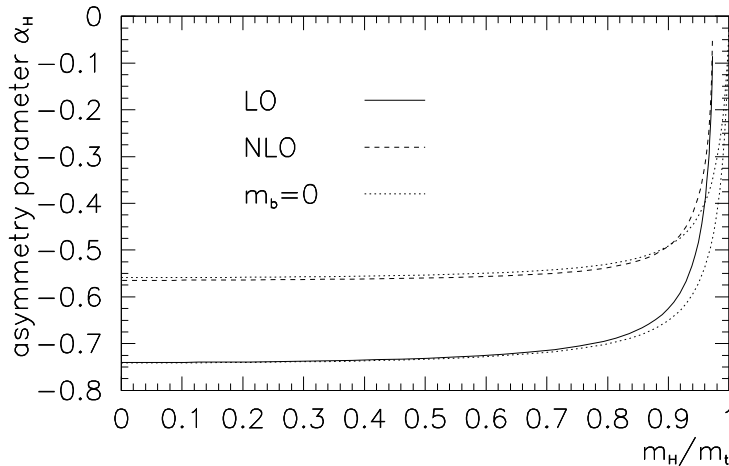


Figure 9: Asymmetry parameter α_H for model 2 with $m_b = 4.8 \text{ GeV}$ and $m_t = 175 \text{ GeV}$ (LO: full line, NLO: dashed line) as function of m_{H^+}/m_t and $\tan\beta = 10$. The barely visible dotted lines show the corresponding $m_b \rightarrow 0$ curves.

11 Goldstone Equivalence Theorem

Consider the decay $t \rightarrow b + J_\mu^+(q^2)$ where the current $J_\mu^+(q^2)$ can be thought of as representing an off-shell W^+ containing spin 1 and spin 0 pieces. Taking $q^\mu = (q_0; 0, 0, |\vec{q}|)$ the longitudinal polarization vector of the spin 1 piece is given by $\epsilon^\mu(L) = (|\vec{q}|; 0, 0, q_0)/\sqrt{q^2}$ while the scalar polarization vector reads $\epsilon^\mu(S) = q^\mu/\sqrt{q^2}$. In the limit $\sqrt{q^2}/m_t \rightarrow 0$ the longitudinal polarization vector becomes increasingly parallel to its momentum. In fact, one finds $\epsilon^\mu(L) = q^\mu/\sqrt{q^2} + O(\sqrt{q^2}/q_0)$. In this limit the amplitude $A(L)$ dominates over the transverse amplitudes $A(T)$ since $A(T)/A(L) \sim \sqrt{q^2}/q_0$. At the same time one finds $A(S) \sim A(L)$ in this limit. This provides a useful check on the high energy limits of the relevant unpolarized and polarized rate functions.

Next consider the scalar projection of the $t \rightarrow b$ current transition at lowest order. Using the Dirac equation one obtains ($q = p_t - p_b$)

$$\begin{aligned}
 q_\mu \bar{u}_b \gamma^\mu (\mathbb{1} - \gamma_5) u_t &= (p_t - p_b)_\mu \bar{u}_b \gamma^\mu (\mathbb{1} - \gamma_5) u_t \\
 &= \bar{u}_b (m_t (\mathbb{1} + \gamma_5) + m_b u_t (\mathbb{1} - \gamma_5)) u_t.
 \end{aligned}
 \tag{54}$$

The second line of (54) has the coupling structure of a Goldstone boson in the Standard Model. It is a very instructive exercise to follow this argument through to one-loop

order including renormalization [53]. In fact, this generalizes to any order in perturbation theory: the scalar piece of the charged transition current has the coupling structure of a Goldstone boson. Together with the above statement that the longitudinal rate dominates at high energies and that it is equal to the scalar rate in this very limit one arrives at the Goldstone Boson Equivalence Theorem. In the high energy limit the coupling of a gauge vector boson to a fermion current is equivalent to that of a Goldstone boson. This simplifying feature has frequently been used in the literature to dramatically reduce the effort needed in the computation of high energy processes involving vector gauge bosons. For example, the Goldstone equivalence theorem was used in [54] to calculate the bosonic two-loop electroweak radiative corrections to the decay $H \rightarrow \gamma + \gamma$ in the limit of a large Higgs mass. The same approximation was used to calculate the dominant bosonic two-loop electroweak radiative corrections to the decay of a heavy Higgs into pairs of W and Z gauge bosons [55].

As concerns the coupling of charged Higgs bosons in $t \rightarrow b + H^+$ discussed in Sect. 10 the coupling structure of the charged Higgs is equal to that of a Goldstone boson in the Standard Model if one specifies to the so called model 1 with $\cot \beta = 1$ (see e.g. [8]). In this case one has

$$\Gamma_{t \rightarrow b + H^+} \sim \Gamma_{t \rightarrow b + W^+} \quad \text{as} \quad m_{W^+}, m_{H^+}/m_t \rightarrow 0. \quad (55)$$

The same relation holds true for the corresponding polarized top rates. All of the statements made in this section have been explicitly verified using our *NLO* results on $t \rightarrow b + W^+$ [6] and $t \rightarrow b + H^+$ [8].

12 Leptonic Decays of the μ and the τ and Anomalous Helicity Flip Contributions

We have already discussed various aspects of the leptonic decays of the μ and the τ lepton in previous sections. A complete solution to the problem has been given in [3] where, for the first time, all mass and polarization effects have been included at *NLO*. Partial *NLO* results on polarization can be found in [57, 58]. In this section we concentrate on one aspect of the problem, namely on the so-called anomalous contribution that, in the chiral limit, flips the helicity of the final-state lepton at *NLO*.

Collinear photon emission from a massless fermion line can flip the helicity of the massless fermion contrary to naive expectation. This has been discussed in a variety of physical contexts. This is a “ m_e/m_e ” effect where the m_e in the numerator is a spin flip

factor and the m_e in the denominator arises from the collinear configuration. In the limit $m_e \rightarrow 0$ the helicity flip contribution survives whereas it is not seen in massless QED.

We shall discuss this phenomenon in the context of the left-chiral $\mu \rightarrow e$ transition. At the Born term level an electron emerging from a weak ($V - A$) vertex is purely left-handed in the limit $m_e = 0$. Naively, one would expect this to be true also at $O(\alpha)$ or at any order in α because in massless QED photon emission from the electron is helicity conserving. Let us make this statement more precise by looking at the string of γ -matrices between the initial state μ spinor and final state e antispinor of the left-chiral $\mu \rightarrow e$ transition. Using $(1 - \gamma_5) = (1 - \gamma_5)(1 - \gamma_5)/2$, and the fact that in massless QED every photon emission brings in two γ -factors (one from the vertex and one from the fermion propagator) one finds

$$\bar{u}_e \Gamma^{(n)} \gamma^\mu (\mathbb{1} - \gamma_5) u_\mu = \frac{1}{2} \bar{u}_e (\mathbb{1} + \gamma_5) \Gamma^{(n)} \gamma^\mu (\mathbb{1} - \gamma_5) u_\mu, \quad (56)$$

where $\Gamma^{(n)}$ stands for the (even) γ matrix string brought in by the emission of n photons. We have commuted the left-chiral factor $(1 - \gamma_5)$ to the left end where it then projects out the helicity state $\lambda_e = -1/2$ from the electron antispinor thus proving the above assertion.

Let us take a closer look at the anomalous helicity flip contribution in leptonic $\mu \rightarrow e$ decays by considering the unnormalized density matrix element ρ_{++} of the final state electron which is obtained by setting $\cos \theta = 1$ in (38) (remember that G_5 vanishes for $m_e \rightarrow 0$ and $G_6 = 0$ in the Standard Model). One has

$$\frac{d\Gamma^{(+)}}{dx d\cos \theta_P} = \frac{1}{2} \beta x \Gamma_0 \left((G_1 + G_3) + (G_2 + G_4) P \cos \theta_P \right). \quad (57)$$

Contrary to naive expectations one finds non-vanishing right-handed (+) contributions which survive the $m_e \rightarrow 0$ limit when one takes the $m_e \rightarrow 0$ limit of the *NLO* contributions to (57) [3]. In fact, one finds

$$\frac{d\Gamma^{(+)}}{dx d\cos \theta_P} = \frac{\alpha}{12\pi} \Gamma_0 \left(\left[(1-x)^2 (5-2x) \right] - \left[(1-x)^2 (1+2x) \right] P \cos \theta_P \right). \quad (58)$$

The result is rather simple. In particular, it does not contain any logarithms or dilogarithms. The simplicity of the right-handed contribution becomes manifest in the equivalent particle description of μ -decay where, in the peaking approximation, μ -decay is described by the two-stage process $\mu^- \rightarrow e^-$ followed by the branching process $e^- \rightarrow e^- + \gamma$ characterized by universal splitting functions $D_{nf/hf}(z)$ [56]. The symbols *nf* and *hf* stand for a helicity non-flip and helicity flip of the helicity of the electron. In the

splitting process z is the fractional energy of the emitted photon. The off-shell electron in the propagator is replaced by an equivalent on-shell electron in the intermediate state. Since the helicity flip contribution arises entirely from the collinear configuration it can be calculated in its entirety using the equivalent particle description.

The helicity flip splitting function is given by $D_{hf}(z) = \alpha z/(2\pi)$, where $z = k_0/E' = (E' - E)/E' = 1 - x/x'$, and where k_0 is the energy of the emitted photon. E' and E denote the energies of the initial and final electron in the splitting process. The helicity flip splitting function has to be folded with the appropriate $m_e = 0$ Born term contribution. The lower limit of the folding integration is determined by the soft photon point where $E' = E$. The upper limit is determined by the maximal energy of the initial electron $E' = m_\mu/2$. One obtains

$$\begin{aligned}
\frac{d\Gamma^{(+)}}{dx d\cos\theta_P} &= \frac{\alpha}{2\pi} \int_x^1 dx' \frac{1}{x'} \frac{d\Gamma^{\text{Born}^{(-)}}(x')}{dx' d\cos\theta_P} \left(1 - \frac{x}{x'}\right) \\
&= \frac{\alpha}{2\pi} \Gamma_0 \int_x^1 dx' (x' - x) \left((3 - 2x') + (1 - 2x') P \cos\theta_P \right) \\
&= \frac{\alpha}{12\pi} \Gamma_0 \left((1 - x)^2 (5 - 2x) - (1 - x)^2 (1 + 2x) P \cos\theta_P \right), \quad (59)
\end{aligned}$$

which exactly reproduces the result (58).

Numerically, the flip spectrum function is rather small compared to the $O(\alpha_s)$ no-flip spectrum function. However, when averaging over the spectrum the ratio of the $O(\alpha_s)$ flip and no-flip contributions amounts to a non-negligible (-12%), due to cancellation effects in the $O(\alpha_s)$ no-flip contribution.

13 Summary and Concluding Remarks

We have discussed *NLO* corrections to a multitude of polarization observables in different processes including nonzero mass effects. The results are available in compact analytical form. They are ready for use in physics simulation programs which are reliable even at corners of phase space where mass effects become important. Present and planned experiments (TEVATRON Run2, LHC, BELLE, BABAR, τ -charm factories) will be sensitive to these *NLO* Standard Model effects. Standard Model *NLO* corrections to polarization observables are needed as background for possible new physics contributions. Last but not least the *NLO* results are needed for *NLO* sum rule analysis' involving polarization observables. All calculations are based on the same one-loop and tree-graph matrix

elements. Results on rates agree with previous calculations. Results on polarization observables agree with previous calculations where available. We have checked various limits and found agreement with previous mass zero calculations, the Goldstone boson equivalence theorem and the equivalent particle description of the anomalous helicity flip contribution. Because of the various checks and the fact that we have essentially used one set of matrix elements as input to the calculations we feel quite confident that our results are correct.

Acknowledgements: We would like to thank the organizers of this meeting, D. Blaschke, M.A. Ivanov and S. Nedelko for providing a most graceful conference setting. We acknowledge informative discussions and e-mail exchanges with A.B. Arbuzov, F. Berends, W. van Neerven, F. Scheck, K. Schilcher, H. Spiesberger and O.V. Teryaev. We would like to thank B. Lampe, M. Fischer, S. Groote and H.S. Do for their collaborative effort. M.C. Mauser is supported by the DFG (Germany) through the Graduiertenkolleg “Eichtheorien” at the University of Mainz.

References

- [1] P.A. Baikov, K.G. Chetyrkin and J.H. Kühn: Phys. Rev. Lett. **88** 012001 (2002)
- [2] P.A. Baikov, K.G. Chetyrkin and J.H. Kühn: hep-ph/0212299
- [3] M. Fischer, S. Groote, J.G. Körner and M.C. Mauser:
hep-ph/0203048 (2003), to be published in Phys. Rev. D
- [4] M. Fischer, S. Groote, J. G. Körner, B. Lampe and M. C. Mauser:
Phys. Lett. B **451** 406 (1999)
- [5] M. Fischer, S. Groote, J.G. Körner and M.C. Mauser:
Phys. Rev. D **63** 031501 (2001)
- [6] M. Fischer, S. Groote, J.G. Körner and M.C. Mauser:
Phys. Rev. D **65** 013205 (2002)
- [7] H.S. Do, S. Groote, J.G. Körner and M.C. Mauser: Phys. Rev. D **67** 091501 (2003)
- [8] J.G. Körner and M.C. Mauser: hep-ph/0211098

- [9] M. Fischer, S. Groote, J.G. Körner and M.C. Mauser: Phys. Lett. B **480** 265 (2000)
- [10] M. Fischer, S. Groote, J.G. Körner and M.C. Mauser:
 “Inclusive decays $\Lambda_b \rightarrow X_c + D_s^{(*)}$ at $O(\alpha_s)$ including Λ_b
 and D_s^* polarization effects”, to be published
- [11] S. Groote, J.G. Körner and J.A. Leyva: Phys. Rev. D **56** 6031 (1997)
- [12] J.G. Körner, A. Pilaftsis and M.M. Tung: Z. Phys. C **63** 575 (1994)
- [13] S. Groote, J.G. Körner and M.M. Tung: Z. Phys. C **70** 281 (1996)
- [14] S. Groote and J.G. Körner: Z. Phys. C **72** 255 (1996)
- [15] S. Groote, J.G. Korner and M.M. Tung: Z. Phys. C **74** 615 (1997)
- [16] A. Brandenburg, M. Flesch and P. Uwer: Phys. Rev. D **59** 014001 (1999)
- [17] V. Ravindran and W.L. van Neerven: Phys. Lett. B **445** 214 (1998);
 Nucl. Phys. B **589** 507 (2000)
- [18] A. Czarnecki, M. Jezabek and J.H. Kühn: Nucl. Phys. B **351** 70 (1991)
- [19] A. Czarnecki, M. Jezabek, J.G. Körner and J.H. Kühn:
 Phys. Rev. Lett. **73** 384 (1994)
- [20] A. Brandenburg: Phys. Lett. B **388** 626 (1996)
- [21] G. Mahlon and S. Parke: Phys. Lett. B **411** 173 (1997)
- [22] W. Bernreuther, A. Brandenburg, Z.G. Si and P. Uwer:
 Phys. Rev. Lett. **87** 242002 (2001)
- [23] W. Bernreuther, A. Brandenburg, Z.G. Si and P. Uwer:
 Phys. Lett. B **509** 53 (2001)
- [24] S. Parke and Y. Shadmi: Phys. Lett. B **387** 199 (1996)
- [25] S. Groote, J.G. Körner and J.A. Leyva: Phys. Lett. B **418** 192 (1998)
- [26] M.M. Tung, J. Bernabeu and J. Penarrocha: Phys. Lett. B **418** 181 (1998)

- [27] J.G. Körner, G. Kramer, G. Schierholz, K. Fabricius and I. Schmitt:
Phys. Lett. B **94** 207 (1980)
- [28] K. Fabricius, I. Schmitt, G. Kramer and G. Schierholz:
Phys. Rev. Lett. **45** 867 (1980)
- [29] A. Brandenburg, L.J. Dixon and Y. Shadmi: Phys. Rev. D **53** 1264 (1996)
- [30] K. Hagiwara, K.i. Hikasa and N. Kai: Phys. Rev. Lett. **47** 983 (1981)
- [31] K. Hagiwara, K.i. Hikasa and N. Kai: Phys. Rev. D **27** 84 (1983)
- [32] K. Hagiwara, K. i. Hikasa and N. Kai: Phys. Rev. Lett. **52** 1076 (1984)
- [33] J.G. Körner, B. Melic and Z. Merebashvili: Phys. Rev. D **62** 096011 (2000)
- [34] K. Hagiwara *et al.* [Particle Data Group Collaboration]:
Phys. Rev. D **66** 010001 (2002)
- [35] W.G. Dharmaratna and G.R. Goldstein: Phys. Rev. D **41** 1731 (1990);
- [36] W. Bernreuther, A. Brandenburg and P. Uwer: Phys. Lett. B **368** 153 (1996)
- [37] W.G. Dharmaratna and G.R. Goldstein: Phys. Rev. D **53** 1073 (1996)
- [38] J.G. Körner, G. Schuler, G. Kramer and B. Lampe:
Z. Phys. C **32** 181 (1986) 181
- [39] J. C. Pati and C. H. Woo: Phys. Rev. D **3** 2920 (1971)
- [40] J.G. Körner: Nucl.Phys.**32** 282 (1970)
- [41] J.H. Kühn, A. Reiter and P.M. Zerwas: Nucl. Phys. B **272** 560 (1986)
- [42] J.G. Körner and G.A. Schuler: Z. Phys. C **46** 93 (1990)
- [43] A. Faessler, T. Gutsche, M.A. Ivanov, J.G. Körner and V.E. Lyubovitskij:
Eur. Phys. J. directC **418** (2002)
- [44] I. Dunietz, H. R. Quinn, A. Snyder, W. Toki and H. J. Lipkin:
Phys. Rev. D **43** 2193 (1991)

- [45] G.J. Gounaris and J.E. Paschalis: Nucl. Phys. B **222** 473 (1983)
- [46] K. Schilcher, M.D. Tran and N.F. Nasrallah, Nucl. Phys. B **181** 91 (1981),
Erratum *ibid.* B **187** 594 (1981)
- [47] C. Bauer and H. S. Do: Comput. Phys. Commun. **144** 154 (2002)
- [48] A. Denner and T. Sack: Nucl. Phys. B **358** 46 (1991)
- [49] H.S. Do, S. Groote, J.G. Körner and M.C. Mauser: to be published
- [50] Future Electroweak Physics at the Fermilab Tevatron: Report of the TeV2000 Group,
edited by D. Amidei and R. Brock, Fermilab-Pub-96/046,
<http://www-theory.fnal.gov/TeV2000.html>
- [51] S. Weinberg: “The Quantum Theory Of Fields. Vol. 1: Foundations,”
(Cambridge University Press, Cambridge 1995)
- [52] S. Groote, J.G. Körner: “Analytical results for $O(\alpha_s)$ radiative corrections
to $e^+e^- \rightarrow \bar{t}t^\dagger$ up to a given gluon energy cut”, to be published
- [53] A. Czarnecki and S. Davidson:
Proceedings of the Lake Louise Winter Institute, 330 (1993)
- [54] J.G. Körner, K. Melnikov and O.I. Yakovlev: Phys. Rev. D **53** 3737 (1996)
- [55] A. Frink, B.A. Kniehl, D. Kreimer and K. Riesselmann:
Phys. Rev. D **54** 4548 (1996)
- [56] B. Falk and L.M. Sehgal: Phys. Lett. B **325** 509 (1994)
- [57] W.E. Fischer and F. Scheck: Nucl. Phys. B **83** 25 (1974)
- [58] A.B. Arbuzov: Phys. Lett. B **524** 99 (2002)